Chapter 13 Microstructure Evolution under Irradiation

13.1 Introduction

As shown in Chapter 12, irradiation with energetic particles creates a population of point defects and defect clusters issuing from the debris of the displacement cascades. After they are created, stable point defects can migrate thermally, and eventually react - that is, be absorbed, annihilated or cluster - with other point defects, or with fixed defect *sinks* that can absorb defects and defect clusters-, such as dislocations, grain boundaries, bubbles and voids.

Because of the high rates of defect generation relative to the concentration of point defects that can be sustained in the lattice, a large fraction of the defects created by displacement damage are constantly annihilated at sinks under irradiation. Since the defects must migrate through the material to arrive at sinks, one of the main effects of irradiation is to cause persistent and significant defect fluxes that permeate the material while it is subjected to the energetic particle flux. One speaks of a "vacancy wind" or an "interstitial wind", because it is the *motion* of the defects and the persistence of these high defect fluxes, rather than higher concentrations of the point defects themselves, that most strongly impact the macroscopic properties of the material.

The interactions of the defects and the defect fluxes with the material microstructure are at the origin of the irradiation-induced processes of microstructural evolution that cause the macroscopically-measurable irradiation effects. These in turn can affect material performance, for example by changing mechanical properties, material dimensions, or causing phase transformations. In ceramic nuclear fuel, point-defect interactions with fission-gas bubbles strongly affect fuel behavior (Chap. 20). In metals, microstructure evolution is the basis for changes in mechanical properties (Chap. 26), increases in corrosion and stress corrosion cracking susceptibility (Chap. 25) and for dimensional instability (Chapts. 19 and 27).

The relevant physical processes and the rate-theory methodology that permits quantitative description of microstructure evolution under irradiation are presented in this chapter.

13.2 Microstructure Evolution under Irradiation

Figure 13.1 illustrates the processes occurring during exposure of a solid to neutron irradiation that can lead to an evolution of the microstructure. In the upper left-hand corner a *displacement cascade* creates a number of defects and defect clusters (1). The large number of displacements in the cascade can cause new phases to appear where the cascade hits (e.g. precipitation, disordering, amorphization), sometimes involving the overlap of two or more cascades (2). The vacancy-rich core in the cascade may collapse into a dislocation loop (3) or remain as a *depleted zone* (1). After intra-cascade clustering and defect interaction has produced the final defect configuration (Chap. 12, see also reference [1]) the remaining isolated defects and defect clusters can then migrate to other defect clusters, dislocation loops, voids and to pre-existing lattice defects, such as the as-fabricated dislocation network, grain boundaries and fission-gas bubbles in ceramic nuclear fuel. Voids are a nearly-spherical cluster of vacancies (Chap. 19) and loops are dislocations formed by a planar cluster of either vacancies or interstitials (Sect. 7.2.6). The interaction of the point defects with the sink structure creates a steady-state concentration of defects that is higher than the equilibrium concentration found in the absence of the irradiation flux (4).

Vacancies and interstitials react with each other by *recombination* (5) whereby both defects disappear and the perfect crystal structure is restored locally. The recombination reaction may be enhanced by trapping of defects at solutes (6). Point defects may also interact with defects of the same type, forming defect clusters (7). Defect clustering and absorption in the material alters the original microstructure, creating *voids* and *loops*. The sink density and strength of the material are continually modified during irradiation.

As shown in Fig. 13.1, interstitials and vacancies may be absorbed at extended sinks, such as the original network dislocations or dislocation loops (8), voids (9), incoherent precipitates (10) and grain boundaries (11). Interaction of point defects with solute atoms (12) may cause solute enrichment or depletion in the vicinity of grain boundaries (13), creating local solute supersaturations which can lead to precipitation of new phases (14). At the same time, cascade atomic mixing drives atoms of pre-existing precipitates back into solid solution in the matrix (15). Absorption of the defects by dislocations can cause *dislocation climb*, which is one of the mechanisms of irradiation creep (16).

Figure 13.1 includes a mix of "athermal" processes (i.e., rates independent of temperature) such as (2) and (15) and thermally-activated processes such as (5), (7) and (8). Microstructural evolution is seen to be a mixture of processes that:

(i) depend on long-range thermal migration, such as defect- assisted dislocation climb
(ii) depend on short-range atomic rearrangements
(iii) are completely athermal.

Consequently, the effects of radiation on the microstructure depend on the balance between the formation of radiation damage and the thermal annealing of such.

The potential energy stored in the material during irradiation is converted to thermal energy in defect-defect and defect-sink reactions. The stored energy then is released as lattice thermal vibrations or phonons. The recombination of interstitials and vacancies is the most obvious example, as it releases about 5 eV. Also reactions such as divacancy formation and defect absorption at dislocations convert potential energy to thermal energy.

The energies of the nuclear particles (neutrons, accelerated ions, fission fragments, beta particles and gamma rays) passing through the material are so high compared to the thermal energy of solids that processes that would not occur from thermal energy are enabled under irradiation. This includes irradiation-induced precipitate dissolution and amorphization.

Finally, all of the above processes shown in Fig.13.1 occur in parallel, so they compete and interact with each other. For example, the absorption of point defects by sinks, cause the sinks to grow, thereby increasing sink strength, and reducing point-defect recombination.

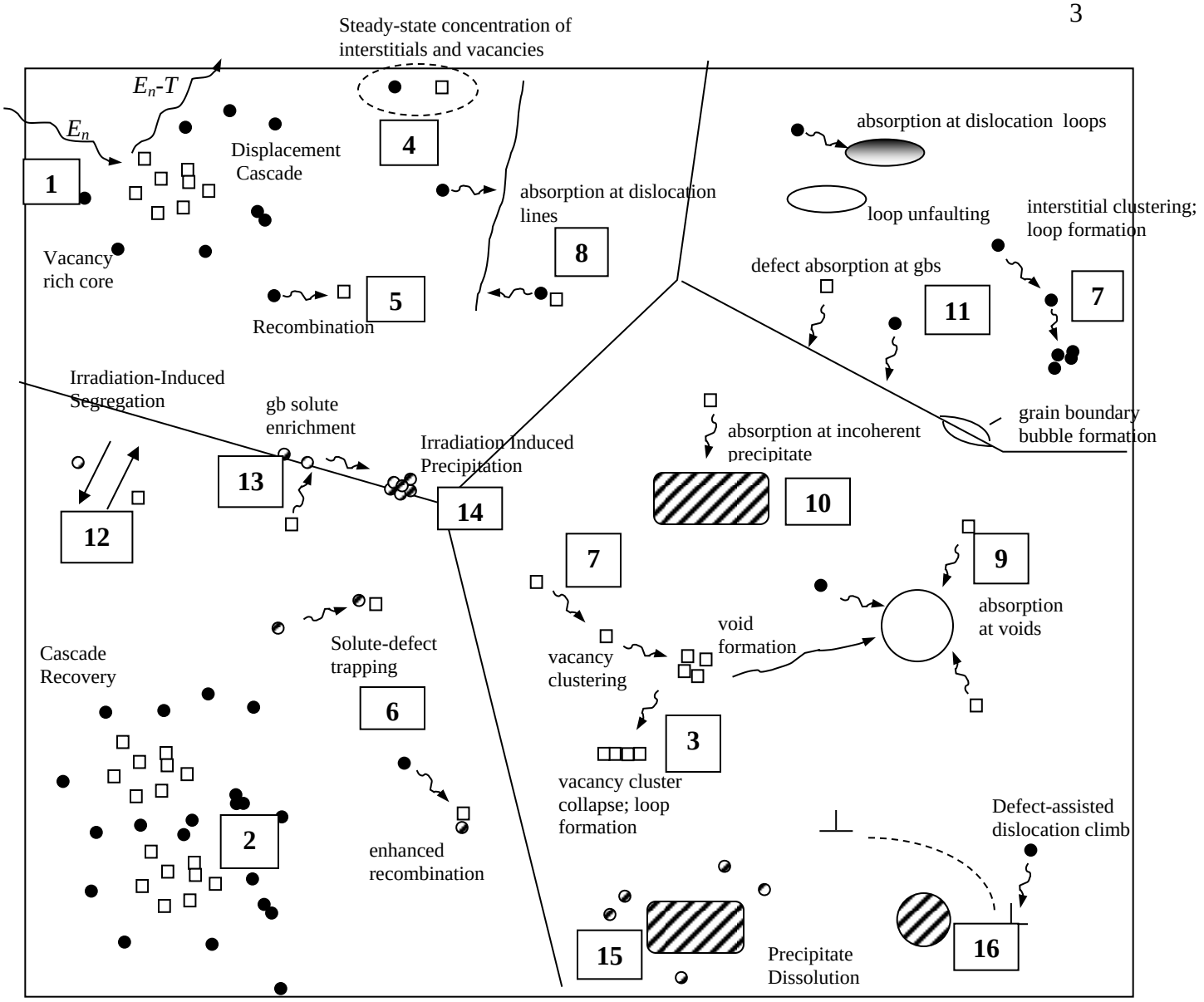

Figure 13.1 : **Point defect processes in irradiated materials**

Mean-Field Reaction Rate theory (hereafter simply rate theory) is an effective tool for treating the complex phenomena described above and is the subject of the remainder of this chapter. In this model the microstructure is *homogenized* so that the kinetic equations become spatially-independent, although spatial correlation of damage can be very important. Even if defects are completely free after a cascade cools, the probability that a vacancy interacts with the interstitials formed in the same cascade is considerably higher than with other interstitials, so that the recombination is *correlated*. Also, although in the simple rate theory formulation an *isotropic* solid is assumed for many phenomena (such as irradiation growth, see Chap. 27) the crystallographic distribution of damage and annealing is often crucial.

13.3 Rate Theory of Defect Evolution under Irradiation

The complex interactions of point defects with the microstructure shown schematically in Fig. 13.1 are difficult to model explicitly, especially in the vicinity of the extended defects, where point-defect gradients exist. In the *rate-theory* formulation [2-5], the bulk defect concentrations, reaction rates and sink strengths are *averaged* over the material, in effect "smearing them out" so that the whole solid is homogeneous. Note that in some situations hybrid schemes can also be used, in which some spatial dependence to an outside sink such as a free surface can be preserved (see Eqs. (13.76) and (13.77) and problem 3).
The *homogenization* approach used in this chapter requires solving the spatially dependent differential equations for point defect reactions with other defects and fixed sinks in an effective unit cell and applying the volume averaged rate over the whole solid. Reaction rates of point defects with other defects and with extended sinks are calculated taking into account the local geometry of these interactions. These locally-calculated defect-sink reaction rates are combined with the sink densities and defect generation rate, to obtain equations describing the variation of the microstructure in terms of these rate processes. These equations are then used to calculate the concentrations of defects and the consequent microstructural evolution for different irradiation conditions.

13.3.1 Basic Rate Theory Assumption

In the classical *rate-theory* model (see also Sect. 20.5.4), the point defect reactions are modeled as first-order chemical reactions, such that the rate of reaction between species *j* and species *i* per matrix atom is

$$K_{ij}\, C_i\, C_j \tag{13.1}$$

where C_i and C_j are the concentrations (site fractions) of *i* and *j* atomic species defined as the ratio of the number of a particular atomic species to the number of sites for that species in the matrix of the material. The reaction rate between atomic species *i* and *j* is characterized by a *rate constant* K_{ij} (s^{-1}), which is independent of the defect concentration and generation rate, but could be dependent on temperature, defect geometry, migration path, etc.

For defect-sink interactions the reaction rate is written in terms of the *sink strength* for the absorption of atomic species *j* by sink S, denoted by $k^2_{j,S}$ (cm^{-2})

$$reaction \quad rate = k_{j,S}^2 D_j C_j \ (\text{s}^{-1}) \tag{13.2}$$

where D_j is the diffusion coefficient for species *j*. The square indicates that the rate constants for defect absorption into sinks are always positive.

Defect-defect reactions

In defect-defect reactions, whether clustering or recombination, the nature of the defect is significantly altered. For example a divacancy is formed from two vacancies, or point defects are completely eliminated when recombination occurs. Some of the more important defect-defect reactions are written in chemical-reaction form:

vacancy-self interstitial atom (SIA) recombination:

$$V + I \xrightarrow{K_{IV}} \text{null} \tag{13.3}$$

divacancy formation *:*

$$V + V \xrightarrow{K_{VV}} V_2 \tag{13.4}$$

vacancy clustering:

$$V + V_2 \xrightarrow{K_{V-V_2}} V_3 \tag{13.5}$$

Di-SIA formation

$$I + I \xrightarrow{K_{II}} I_2, \tag{13.6}$$

SIA Clustering:

$$I + I_2 \xrightarrow{K_{I-I_2}} I_3 \tag{13.7}$$

Defect-fixed sink reactions

Alternatively, the point defect disappears by absorption into a fixed *sink*, which is the generic term for larger features, including spherical defects such as a bubbles, pores and voids, (*cavities* in general), line defects, of which the only example is a dislocation, and planar defects, including grain boundaries and free surfaces.

When point defects are absorbed into these larger features, the sink retains its character, although slightly modified. For example, the absorption of a vacancy into a 100-vacancy void does not appreciably alter the void beyond a very small radius change.

These reactions are written in general as

$$j + \text{sink} \xrightarrow{k_{j,S}^2} \text{"modified" sink} \tag{13.8}$$

In this class of reactions, point defect *j* vanishes and the sink is slightly modified. Examples are:

- arrival of an interstitial at a free surface; the interstitial disappears as a separate entity and adds to a pre-existing ledge of atoms or creates an adatom on the surface.

- fission-gas atom absorption by a bubble causes a slight increase in bubble volume and gas pressure in the cavity
- pickup of an interstitial atom by a void; the void shrinks by one atomic volume

The rate of a point defect-sink reaction per matrix atom is expressed by Eq. (13.2) recalled here:

$$\text{rate per matrix atom} = k_{j,S}^2 D_j C_j$$

Where D_j is the diffusion coefficient of atomic species j and $k_{j,S}^2$ is the sink strength of the extended-sink S (cm^{-2}). The concentrations can be either volumetric (c_j number of atomic species per unit volume) or site fraction (C_j in number per atom). The two units are related by:

$$C_j = c_j \Omega \tag{13.9}$$

where Ω is the the atomic volume of the matrix atoms. Most of the radiation damage literature utilizes site-fraction units in point-defect reaction rate expressions, and this convention is followed in this book.

13.4 Reaction Rate between Point Defects

In this section the individual rates of defect reactions both between point defects in the material are calculated for divacancy and interstitial-vacancy recombination.

Reaction rates between point defects are calculated by identifying the set of lattice sites around one defect which, if occupied by the other defect, assures reaction. The number of such sites is termed a *combinatorial number*, generically designated as *Z*.

The combinatorial number Z increases as the energy released in the defect-defect reaction increases. For example, for divacancy formation, the number of assured-reaction sites is equal to the number of nearest neighbors multiplied by the number of second nearest neighbors from where a jump can occur – (see Fig. 13.3). In contrast, for interstitial-vacancy recombination the strain fields extend further and therefore the defect-defect reaction can occur at larger distances, which entails a larger interaction volume.

The rate of reaction is equal to the probability of finding a defect at one jump distance from one or more combinatorial sites times the probability that a reaction jump occurs.

13.4.1.Divacancy formation

The initial step of vacancy-cluster formation is the production of a divacancy from two vacancies, reaction (13.4). This reaction proceeds preferentially from left to right because the formation of a divacancy from two isolated single vacancies reduces the energy of the system by the difference between twice the formation energy of a vacancy and the formation energy of a divacancy (Fig.13.2).

The probability per unit time that a vacancy in one of the second-nearest-neighbor positions to a *particular* vacancy jumps into a nearest-neighbor position (thus forming a divacancy) is P_{VV}. The rate of divacancy formation per atom is

$$P_{VV}\ C_V \tag{13.10}$$

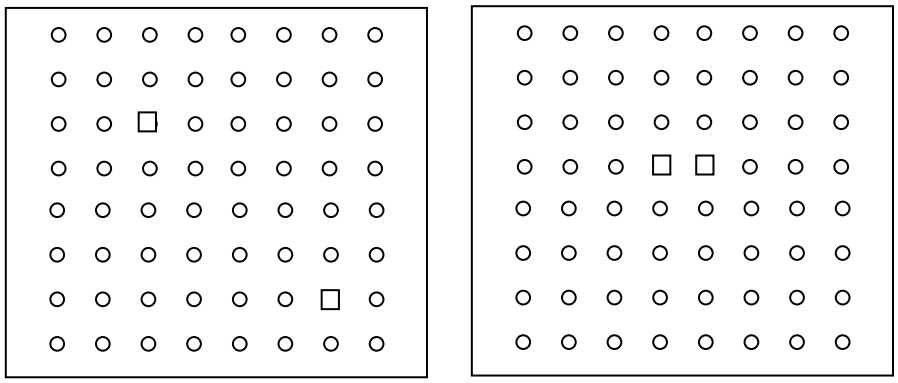

$E=2\ E_f^V$ $E'=E_f^{2V}$

Figure 13.2: The formation of a divacancy. The total energy of the system decreases with divacancy formation

where P_{vv} is the product of the number of favorable configurations for a jump, the vacancy site fraction C_V and the jump frequency:

$$P_{VV} = \beta z_2 C_V\ w \tag{13.11}$$

where β is the number of nearest neighbors to the particular vacancy, z_2 is the number of lattice positions around the ring of nearest neighbor *from which a second vacancy can jump into a nearest-neighbor site*. Then $z_2\ C_V$ vacancies are available around a particular target nearest-neighbor site to a vacancy to perform a jump that creates a divacancy. For all vacancies in a mole of matrix atoms, the rate of divacancy formation per matrix atom is then

$$\beta z_2\ C_V^2\ w \tag{13.12}$$

From chapter 5, the jump frequency is

$$w = \upsilon\ e^{-\frac{E_m^V}{k_B T}} \tag{13.13}$$

From the rate-theory formalism expressed in Eq. (13.1) the reaction-rate constant is:

$$K_{VV} = \textit{combinatorial}\ \text{number} \times \text{jump probability} = \beta\ z_2\ w = Zw \tag{13.14}$$

or, with Eq (5.25):

$$K_{VV} = \frac{6 Z D_V}{\beta \lambda^2} \tag{13.15}$$

Where λ is the vacancy jump distance (approximately equal to a lattice constant).

Example #1: Divacancy formation rate in the fcc lattice
Figure 13.2 shows the relevant geometrical configuration needed to calculate the combinatorial number for divacancy formation for the fcc lattice, There are twelve nearest neighbor sites in the fcc lattice and thus $\beta = 12$. For each of the nearest neighbor sites there are twelve nearest- neighbor sites. Of these, one is the original vacancy and five are shared with that vacancy so jumps from these sites are eliminated. The remaining seven are sites from which a jump into the nearest neighbor site would create a divacancy from two separate vacancies, so $z_2 = 7$ and the combinatorial number for divacancy formation in the fcc lattice is 84.

Since both vacancies are equally mobile, the rate is twice as high, **or 168.**

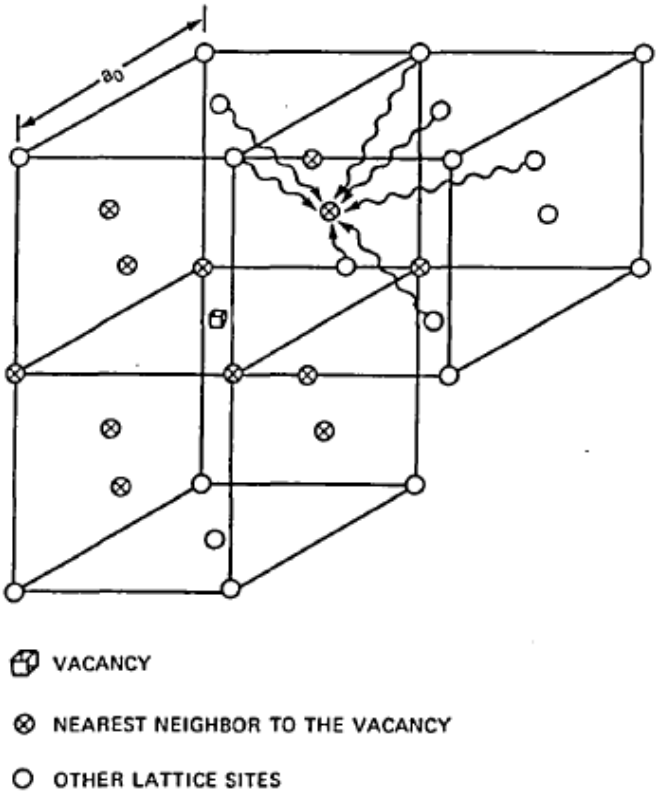

Fig. 13.3 Divacancy formation in the fcc structure. [6]

Similar calculations can be performed for other crystal lattice structures, such as bcc, sc and hcp. For anisotropic structures, migration energies can be directionally dependent, so it is necessary to identify the correct migration direction and migration paths, but the same principles apply.

13.4.2. Point-Defect Recombination

The rate constant for vacancy -interstitial recombination is calculated in a similar fashion to the formation of divacancies from single vacancies. Because vacancy-interstitial recombination results in a perfect lattice (defects are annihilated), the amount of energy released is considerably higher than that from divacancy formation, so the number of assured recombination sites is higher than the geometrical size of the defects. As seen in Chap. 12, if an interstitial enters a region around the vacancy called the *recombination volume*, mutual annihilation occurs without need for thermal motion. Because the energy released upon recombination is quite high (~5eV), the region around the vacancy whence athermal recombination can occur can comprise many hundreds of atoms

By analogy with the divacancy derivation, section 13.4.1,

Recombination rate = number of favorable configurations × jump probability = $P_{IV}w$ (13.16)

The number of favorable configurations is computed in a manner similar to that for divacancy formation but in a less straightforward way because of the complex geometry. In this case, the critical rate-determining step is the jump from the outside to the inside of the recombination volume. Thus z_1 is number of sites within the recombination volume but next to its outer surface and z_2 is the number of sites just outside the recombination volume from which a jump could occur to each of the z_1 sites.

The number of favorable configurations for a recombination jump is then

$$P_{IV} = C_V z_1 z_2 C_I = C_V Z_{IV} C_I \tag{13.17}$$

The jump frequency is the sum for the two defects, $w=w_I+w_V \sim w_I$. In metals the interstitial migration energy is normally much lower than the vacancy migration energy, and so $w_I >> w_V$. Since the three-dimensional configuration of sites z_1 and z_2 is complicated and crystal-structure dependent, we give a two- dimensional example below.

Example # 2: Recombination region
The recombination rate constant is calculated for the schematic 2D recombination volume configuration shown below. The migration energies and interatomic potentials are such that any interstitial entering the dotted line would athermally recombine with the vacancy in the center (the definition of recombination volume). Only the interstitial is mobile. In the figure below, one could imagine the interstitial replacing any one of the atom locations right outside the recombination volume.

Figure 13.4 shows three different types of recombination sites (labeled 1, 2 and 3), totaling four of each for a total of $z_1 = 12$. As seen in the figure, the number of next-nearest-neighbor sites is different for each recombination site. For type 1, there are four; for type 2 sites, there are two and for type 3 sites only one.

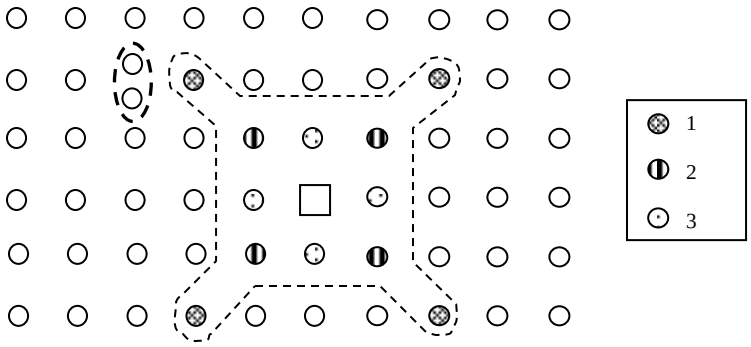

Figure 13.4: Two dimensional configuration of the athermal recombination volume around a vacancy (dotted line), showing the three different types of sites. A dumbbell interstitial (outlined) is shown about to enter the recombination volume

The combinatorial number is thus 4× (4+2+1)=28 possible jumps leading to recombination and thus K_{IV} =28w. Clearly, for a 3D case, the total possible number of jumps would be much higher, leading to a higher value of the combinatorial number.

In the general case, the total number of favorable configurations is given by

$$P_{IV} = C_I C_V \sum_{all\, j} z_{2j} \tag{13.18}$$

where j = all sites z_1, which are nearest neighbor to the defect .

Thus the recombination reaction rate is

$$C_I\ C_V w_I \sum_{all\ j} z_{2j} = Z_{IV} C_I\ C_V w_I \tag{13.19}$$

and the recombination rate constant is $K_{IV} = Z_{IV} \times w_I$, where Z_{IV} is the combinatorial number (also called the *recombination number*). The values of the summation $Z_{IV} = \sum_j z_{2j}$ over all possible configurations can range from 50-500. Typical recombination numbers could be on the 100s, but each crystal structure has its own recombination volume, which tends to extend along close packed directions. The recombination rate constant is

$$K_{IV} = \frac{Z_{IV}(D_I + D_V)}{\lambda^2} \cong \frac{Z_{IV} D_I}{\lambda^2} \tag{13.20}$$

λ is the diffusive jump distance. The final approximation assumes $D_I >> D_V$.

The difference in the formulation above from that in Eq. (13.14) stems from the fact that not all sites at the edge of the recombination volume are equivalent, as is the case for di-vacancy recombination.

13.5 Point-Defect Reactions with Extended Sinks

An important feature of point-defect behavior in both metals and actinide oxides under irradiation is their removal from the matrix by diffusion and annihilation at defect sinks in the microstructure. Many common sinks are spherical, such as voids and helium bubbles in a metal (Chap. 19) and fission-gas bubbles in oxide fuel. In addition, dislocations in metals are *line sinks* for both vacancies and interstitials and grain boundaries are *surface sinks* for point defects and for diffusing rare-gas atoms. The determination of the vacancy and interstitial absorption rates in these extended sinks as functions of the concentrations of the point defects is an important step in determining the material behavior under irradiation.

To a first approximation, the voids, bubbles and dislocations are "perfect" sinks for the point defects. In a perfect sink, all defects stick completely to the sink, i.e. the sinks acts as a black hole. In the analysis, the point-defect concentration at the surface of these sinks is zero, sinks so the reaction rate is given by Eq (13.2), where C_j is the volume-average site fraction of point defect j in the solid and the rate of point defect absorption is

$$DC_j k_{S,j}^2 \tag{13.21}$$

The *sink strengths* $k_{S,j}^2$ *(units of* cm^{-2}*)*are derived for spherical and line sinks. D is the diffusivity of the point defect, The rates are calculated by using the geometric shape of the sink and assuming that point-defect diffusion limits the defect ingress rate into the sink.

The sinks are considered to be inexhaustible, i.e. absorption of defects does not change the sink strength. Strictly speaking this is not the case, since the strength of extended sinks can change during irradiation. For example, an incoherent precipitate with a larger volume than the matrix has a volume mismatch with the matrix, and is a sink for vacancies, since vacancy absorption helps eliminate strain energy. However, as vacancies are absorbed, such mismatch decreases, until the precipitate is no longer a net vacancy sink. These effects are not considered in the following sections.

13.5.1 Sink Strengths: Isolated Sinks

Dislocation Sink

Point defects are absorbed at dislocations because there is a net elimination of lattice strain energy as a result of this reaction. Defect absorption eliminates the defect and causes a small jog to appear in the dislocation line (the additional energy on the dislocation line from the jog is much smaller than the vacancy formation energy E_v^f so that there is a net decrease in energy upon defect absorption).

Multiple absorptions of one type of point defect cause the dislocation line to climb (see Chap. 7). Absorption of point defects by dislocations is modeled in rate theory as follows:

1. The dislocation distribution is represented by the dislocation density ρ_d. An even distribution of dislocation lines constituted of only one type of dislocation is assumed. In reality, the distribution of dislocations is quite anisotropic and inhomogeneous, and many different types of dislocation exist.
2. There is a region next to the dislocation line, the *dislocation core* (Sect. 7.5), into which defects enter and are invariably captured by the line.
3. The effect of the dislocation line on the concentration of point defects in the matrix diminishes with distance such that at the dislocation unit-cell radius (Eq (7.4)), the concentration of defects is equal to the average bulk concentration.
4. Within the *unit-cell radius* of the dislocation R_{cell}, the defects undergo random walk, with no influence of the dislocation strain field.
5. The rate of absorption of defects is limited by diffusion to the dislocation core

Although dislocations normally form a chaotic tangle in a solid, mathematical analysis requires a highly simplified geometry. To this end, the dislocation population is represented as an array of parallel lines on a square pattern, such as shown in Fig. 13.5. Each infinitely-long line occupies a square parallelepiped, and only this geometry needs to be analyzed. To further simply the problem, the cell is taken as a *cylinder* of the same area as the square, as shown at the top of the drawing. Because the line and its unit cell are infinite in length, the diffusion equation to be solved is:

$$\frac{D}{r}\frac{d}{dr}\left(r\frac{dC'}{d\,r}\right)=-k \tag{13.22}$$

where *C'* is the *spatially-varying* defect site fraction, *r* is the radial distance from the dislocation line and *k* is the net point defect production rate (per matrix atom or molecule site). The production rate is assumed to be constant over $R_d < r < R_{cell}$. The radius R_d is radius of the dislocation core and represents the distance from the dislocation which, if penetrated by a point defect, assures capture of the defect by the line. It is less than 1 nm .

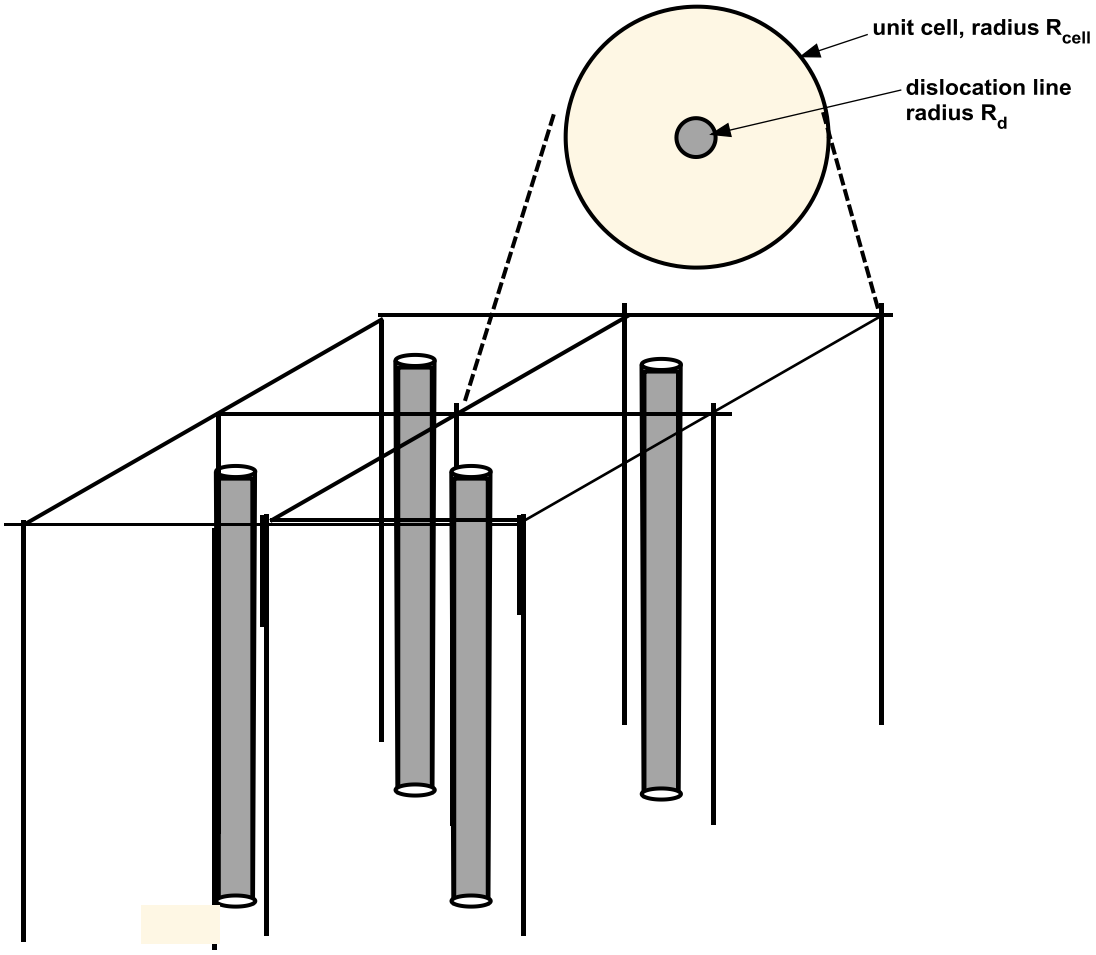

Fig. 13.5 Representation of dislocation lines in a solid

The cell radius R_{cell} is fixed by the dislocation density ρ_d, in units of length of line per unit volume of solid, or cm^{-2}. The reciprocal, $(\rho_d)^{-1}$ is the area per line, or:

$$\pi R_{cell}^2 = \rho_d^{-1} \tag{13.23}$$

So each dislocation has a "claim" on all defects inside "its" cylinder. The dislocation core, radius R_d acts like a perfect sink. This is represented in Fig. 13.6.

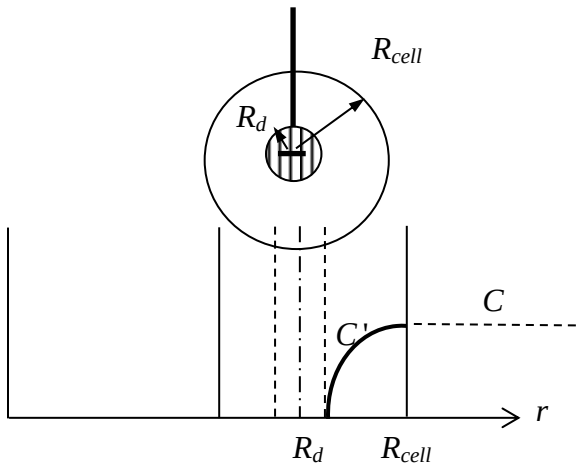

Fig. 13.6: Geometry for the derivation of the reaction rate for defect-dislocation line interaction.

here C is the average atom fraction of point defects in the lattice.

Since the problem is symmetrical in the θ direction and there is no gradient in the z direction, the defect concentration depends only on r. Assuming that the defect generation rate in the cylinder is negligible during the diffusion time of the defect from R_{cell} to R_d, the balance equation in the region associated with the dislocation is:

$$\frac{1}{r}\frac{d}{dr}\left(r\frac{dC'}{dr}\right)=0 \tag{13.24}$$

to be solved with the following boundary conditions

$$\begin{aligned} &\text{(i)} \quad C'(R_d) = 0 \\ &\text{(ii)} \quad C'(R_{cell}) = C \end{aligned} \tag{13.25}$$

Integrating equation (13.24) and applying the boundary conditions yields:

$$\frac{C'(r)}{C}=\frac{\ln(r/R_d)}{\ln(R_{cell}/R_d)} \tag{13.26}$$

Figure 13.7 shows a typical concentration profile around a dislocation according to Eq (13.26).

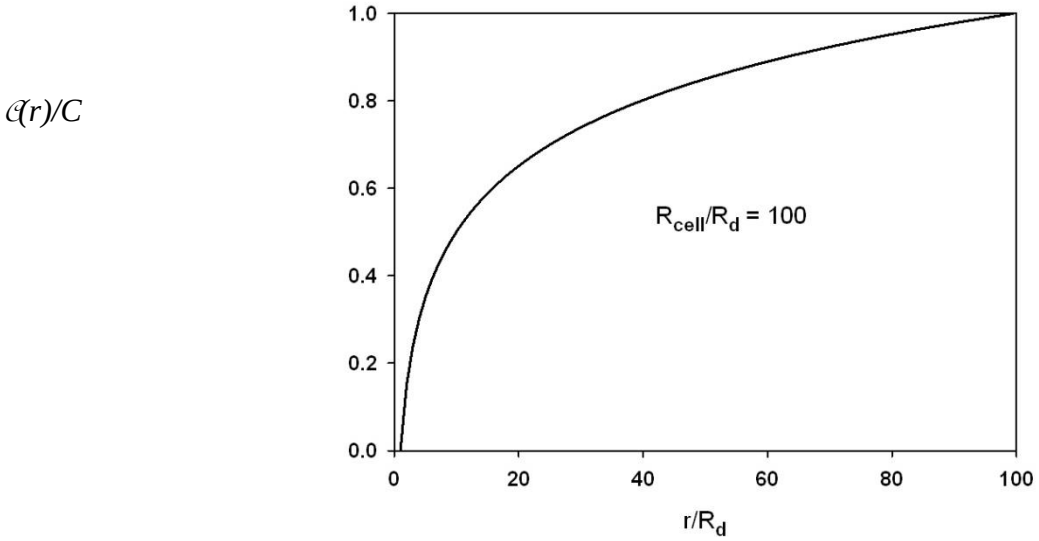

Fig. 13.7 Point-defect concentration distribution around a dislocation line

The defect flux per unit length of dislocation line is then given by:

$$j^{dis} = 2\pi R_d \left[D\left(\frac{dC'}{dr}\right)_{R_d} \right] \tag{13.27}$$

Substituting equation (13.26) into (13.27) we obtain

$$j^{dis} = 2\pi \frac{D\,C}{\ln(R_{cell}/R_d)} \cong zDC \tag{13.28}$$

Since there are ρ_d cm of dislocation line per cm^3, we obtain

$$J^{dis} = j^{dis}\rho_d = z\rho_d DC \tag{13.29}$$

Thus the vacancy flux into dislocations is:

$$J_V^{dis} = j_V^{dis}\rho_d = z_V \rho_d D_V C_V \tag{13.30}$$

This equation has units of s^{-1}, as C is given in atom fraction. For reasonable values of the dislocation core radius and dislocation density, $z_v = \dfrac{2\pi}{\ln(R_{cell}/R_d)} \approx 1$.

For interstitials the flux to dislocations is

$$J_I^{dis} = j_I^{dis}\rho_d = z_I \rho_d D_I C_I \tag{13.31}$$

The assumption of random walk of defects inside the dislocation cylinder is less valid for interstitials which interact more strongly with the dislocation than vacancies do. As evaluated quantitatively in the example below, the interaction factor is z_I ~1.02.

Example #2 Interstitial Bias Factor of Dislocations

To estimate the interaction between dislocations and interstitials we assume that the compressive stress field in a solid near an interstitial interacts with the tensile stress field at the underside of edge dislocations (see Sect. 7.5.2). The initial hole is atomic size, i.e.

$$R_o \approx \Omega^{1/3} \tag{13.32}$$

where Ω is the atomic volume and is expanded to a radius $(1+\varepsilon)\, R_o$ when the interstitial is inserted,.

$$\Delta V = \frac{4}{3}\pi\left[(1+\varepsilon)^3 R_o^3 - R_o^3\right] \approx 4\pi R_o^3 \varepsilon \tag{13.33}$$

Lattice expansion performs work against the hydrostatic component of the dislocation stress field σ_h which leads to an interaction energy

$$E_I = -\sigma_h \Delta V \tag{13.34}$$

From . Eqs (7.6) and (7.8), the hydrostatic stress generated by an edge dislocation is

$$\sigma_h = \frac{1}{3}\left(\sigma_{rr} + \sigma_{\theta\theta} + \sigma_{zz}\right) = -\frac{Gb}{3\pi}\left[\frac{1+\nu}{1-\nu}\right]\frac{\sin\theta}{r} \tag{13.35}$$

Combining equations (13.35) and (13.34) we obtain

$$E_I = \frac{4}{3}\left[\frac{1+\nu}{1-\nu}\right] Gb\varepsilon R_o^3 \frac{\sin\theta}{r} \tag{13.36}$$

According to Eq (13.36), when the interstitial is in the compressive stress field of the dislocations (near the extra half sheet of atoms) the dislocations repels the interstitial while when in the *tensile* stress field of the dislocation ($\pi < \theta < 2\pi$) the interaction is attractive. The interstitial migration in this stress field is biased by this interaction. To obtain the biased flux the interstitial diffusion equation is solved accounting for the force exerted by the dislocation.

To simplify the calculation we set $\sin\theta = -1$ to make the force cylindrically symmetric and combining all other properties in Eq (13.36) into a single constant *B* so that

$$E_I = -\frac{B}{r} \tag{13.37}$$

So that the force exerted by the dislocation on the interstitial is

$$F_I = -\frac{dE_I}{dr} = -\frac{B}{r^2} \tag{13.38}$$

This force creates an inward drift velocity (the migration is no longer random) of $v_{drift} = MF_I$ where *M* is the interstitial mobility. From p.238 of [6] $M = D_I / k_B T$. The drift term modifies Fick's law (written this time in terms of *volumetric* concentration [cm^{-3}]) as

$$j_I = -D_I \frac{dc_I}{dr} + c_I v_{drift} = -D_I \frac{dc_I}{dr} + c_I \frac{D_I}{k_B T} F_I \tag{13.39}$$

which is introduced into the conservation equation as

$$\frac{1}{r}\frac{d}{dr}(r j_I) = 0 \tag{13.40}$$

Substituting Eq (13.39) into (13.40)

$$\frac{d}{dr}\left(r \frac{dc_I}{dr} \right) - \frac{B}{k_B T}\left(\frac{c_I}{r^2} - \frac{1}{r}\frac{dc_I}{dr} \right) = 0 \tag{13.41}$$

This equation is solved with the same boundary conditions as Eq (13.24). However now the interstitial bias factor is given by

$$z_I = 2\pi \left(\int_{R_d}^{R_{cell};} \exp\left(-\frac{B/k_B T}{r} \right) \frac{dr}{r} \right)^{-1} \tag{13.42}$$

In the limit where $B/k_B T << R_d$ (weak interaction) and if $R_{cell} >> R_d$ the integral in Eq (13.42) is approximated as

$$\int_{R_d}^{R_{cell};} \exp\left(-\frac{B/k_B T}{r} \right) \frac{dr}{r} \cong \ln\left(\frac{R_{cell}}{R_d} \right) - \frac{B/k_B T}{R_d} \tag{13.43}$$

so that

$$z_I = 2\pi \left[\ln\left(\frac{R_{cell}}{R_d} \right) - \frac{B/k_B T}{R_d} \right]^{-1} \cong \frac{2\pi}{\ln(R_{cell}/R_d)} \left[1 + \frac{B/R_d k_B T}{\ln(R_{cell}/R_d)} \right] \tag{13.44}$$

The second term in brackets is the bias for interstitials absorbed into dislocations

$$\frac{z_I - z_V}{z_V} = \frac{B/R_d k_B T}{\ln(R_{cell}/R_d)} \tag{13.45}$$

for Cu at 573 K, with G=4 x 10^{10} Pa, b=1.5 x 10^{-10} m, R_o=2.34 x 10^{-10} m, R_d=5x10^{-9} m, R_{cell} =1/$\sqrt{\pi\rho_d}$ = 5.6 x 10^{-7} m, ε=0.02, ν=0.34 we obtain $(z_I - z_V)/z_V$= 0.022.

Because of this difference, dislocations are *biased sinks* for interstitials. From the above by inspection the dislocation sink strengths for vacancies and interstitials are then:

$$k_{I,dis}^2 = z_I \rho_d \tag{13.46}$$

$$k_{V,dis}^2 = z_V \rho_d \tag{13.47}$$

Although the above analysis was derived for straight dislocations, it can also be used for dislocation loops. In this case ρ_d is used, with no consideration of geometry, so that circular dislocations are effectively "straightened out".

Spherical Sinks

Similar arguments for point defect absorption can be made in the case of spherical cavities, such as voids or bubbles uniformly spaced on a cubic lattice (Fig. 13.8). Spherical sinks in solids occur in numerous radiation environments, including fission-gas bubbles in oxide nuclear fuels, as well as voids and helium bubbles in metals generated by fast-neutron irradiation or by ion irradiation in an accelerator.

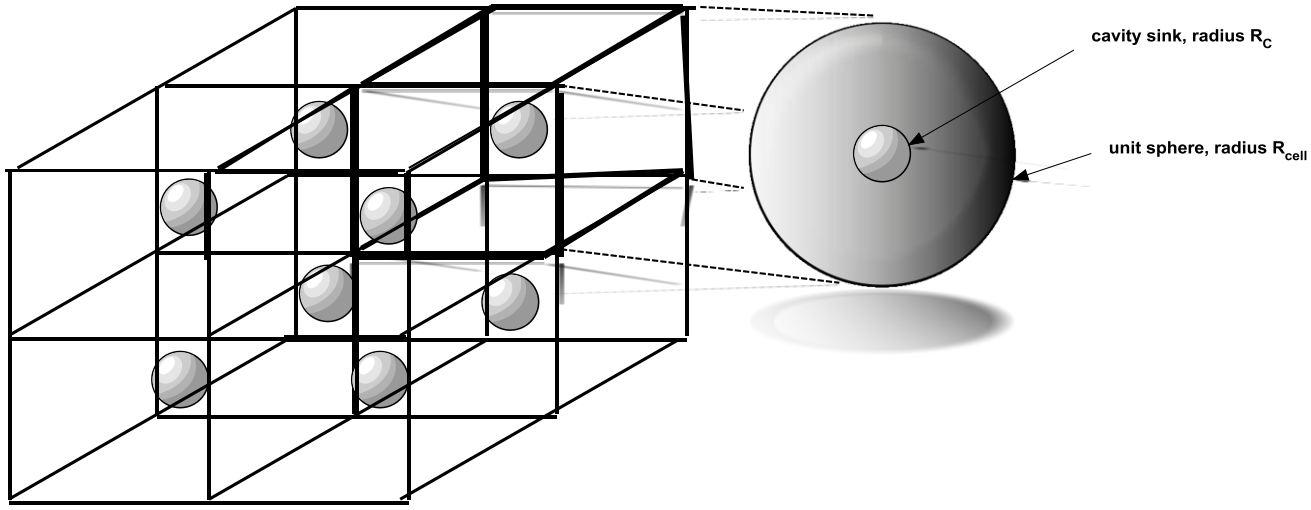

Fig. 13.8 Spherical cavity sinks uniformly distributed in a solid. The cubes are unit cells for each sphere.

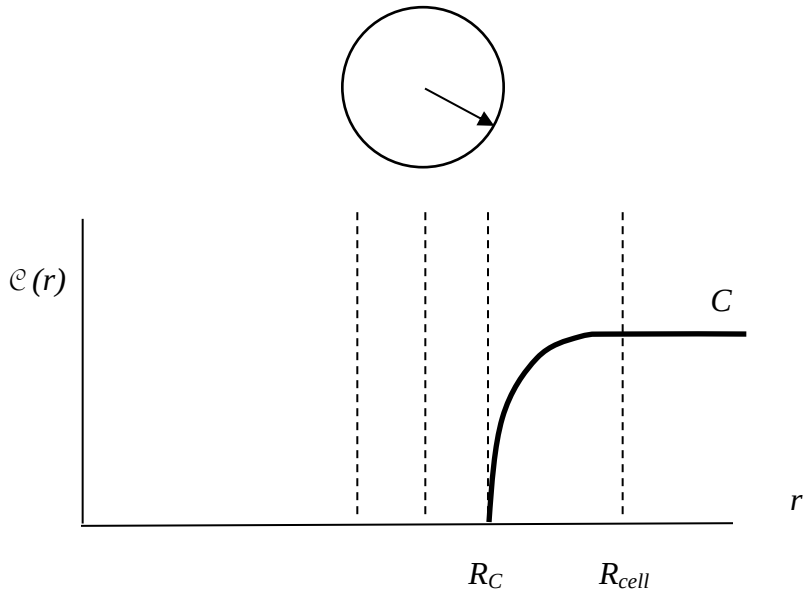

Figure 13.9 Geometry for calculation of defect absorption at voids

In a solid containing N_C cavities per unit volume, the volume associated with each void is equal to $1/N_C$ All defects created within that volume are absorbed into the void. The cell radius is

$$R_{cell} = \left[\frac{3}{4\pi N_C} \right]^{\frac{1}{3}} \tag{13.48}$$

The diffusion of defects to the cavity at the center controls the absorption rate. If the defect generation during diffusion is neglected, the defect concentration depends only on *r*, and the appropriate equation is (See p 212 of Ref. 5 for the same derivation)

$$\frac{1}{r^2}\frac{d}{dr}\left(r^2 \frac{dC'}{dr} \right) = 0 \tag{13.49}$$

with the boundary conditions:

(i) as $dC'/dr = 0$ at $r = R_{cell}$ (by definition of unit cell) (13.50)

(ii) as $r \to R_{cell}, \quad C' \to C$

By definition of the unit cell, the concentration gradient at R_{cell} is zero and the concentration is zero at the cavity surface. The solution of Eq (13.49) is

$$C'(r) = C + \frac{R_C C}{(R_{cell} - R_C)} - \frac{R_C}{(1 - R_C / R_{cell})}\frac{C}{r} \tag{13.51}$$

Where C is the atom fraction far from the sample. If $R_{cell} \to \infty$ we obtain a simpler form

$$\frac{C'(r)}{C} = \left(1 - \frac{R_C}{r}\right) \tag{13.52}$$

and $\frac{dC'}{dr} = \frac{R_C C'}{r^2}$ so that the rate of absorption of defect *j* per cavity is:

$$j_j^C = 4\pi R_C^2 D_j \frac{d\mathcal{C}}{dr} = 4\pi R_C D_j C \tag{13.53}$$

Since there are N_C cavities per unit volume, the rate of vacancy and interstitial absorption into cavities per matrix atom is

$$J_V^C = 4\pi R_C D_V \; C_V \; N_C \tag{13.54}$$
$$J_I^C = 4\pi R_C D_I \; C_I \; N_C$$

This is same as Eq (13.70) of Ref. 5, and the cavity sink strength is

$$k_C^2 = 4\pi R_C N_C \tag{13.55}$$

The same technique can be applied to derive grain boundary and free surface sink strengths (Sect. 13.7).

13.5.2. Sink Strengths for dislocations and voids: Accurate calculation

The sink strength derivations in the two previous sections are normally used in the literature. The derivations assume that migration is isotropic, which has been shown not to be the case [7]. In addition Hayns and others have provided corrections to the sink strengths [8]. For the sake of illustration we show one such correction, namely to the assumption that each sink can be treated in isolation, such that there is no interaction between sinks and that the production rate of the point defects can be neglected. This assumption is removed in the more accurate sink-strength derivations below.

Dislocation Sink

As above the dislocation geometry is simplified to that of Fig. 13.5 so that instead of Eq (13.23), the point-defect balance is:

$$\frac{D}{r}\frac{d}{dr}\left(r\frac{dC'}{dr}\right) = -k \tag{13.56}$$

where *D* is the diffusivity of the mobile point defect, and r is the radial distance from the dislocation line. *k* is the net production rate (per atom or dpa/s) of the point defect considered. The production rate is assumed to be constant over $R_d < r < R_{cell}$. As above the cell radius is fixed by Eq. (13.23).

The boundary conditions for Eq (13.56) are:

$$C'(R_d) = 0 \qquad \text{and} \qquad \left(\frac{dC'}{dr}\right)_{R_{cell}} = 0 \tag{13.57}$$

The solution for the concentration distribution around the line is:

$$C'(r) = \left(\frac{k R_{cell}^2}{2D}\right)\left[\ln\left(\frac{r}{R_d}\right) - \tfrac{1}{2}\left(\frac{r^2 - R_d^2}{R_{cell}^2}\right)\right] \tag{13.58}$$

This solution is recast in terms of the following dimensionless quantities: check units of Θ

$$\eta = \frac{r}{R_d} \qquad \Theta = \frac{C'}{\left[kR_d^2/2D\right]} \qquad \beta = \frac{R_{cell}}{R_d} \tag{13.59}$$

yielding:

$$\Theta(\eta) = \beta^2 \ln(\eta) - \tfrac{1}{2}\left(\eta^2 - 1\right) \tag{13.60}$$

The area-averaged concentration is:

$$C = \frac{1}{\pi(R_{cell}^2 - R_d^2)} \int_{R_d}^{R_{cell}} 2\pi r C'(r) dr \qquad \text{or} \qquad \bar{\Theta} = \frac{2}{\beta^2 - 1} \int_1^{\beta} \eta \Theta(\eta) d\eta \tag{13.61}$$

Substituting Eq (13.60) into Eq (13.61) gives:

$$\bar{\Theta} = \frac{\beta^2}{\beta^2 - 1}\left[\beta^2\left(\ln\beta - \tfrac{3}{4}\right) + 1 - \tfrac{1}{4}\frac{1}{\beta^2}\right] \approx \beta^2\left(\ln\beta - \tfrac{3}{4}\right) \tag{13.62}$$

which is valid for $\beta >> 1$. In most practical situations $\beta > 100$ so that the approximation is valid**.**

Figure 13.10 plots the point-defect distributions around the dislocation line (Eq (13.60)) (solid curves) and the average concentration given by Eq (13.62) (dashed lines). Curves for β values correspond (by Eq (13.59)) to R_d = 0.6 nm and R_{cell} from Eq (13.23) for $\rho_d = 10^8$ cm^{-2} and $\rho_d = 10^{10}$ cm^{-2}. Both of these values are typical of commercial metals and ceramics.

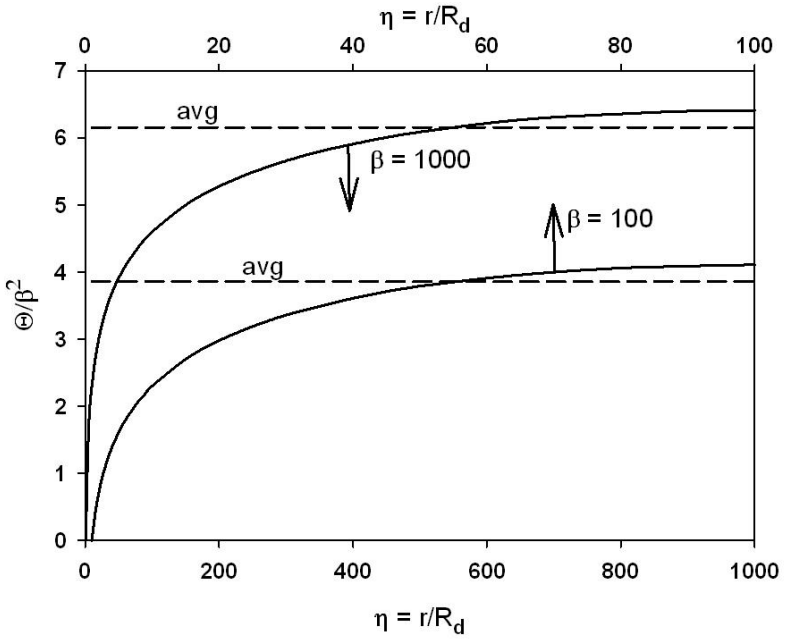

Fig. 13.10 Point-defect concentrations around dislocation lines. Volume-averaged concentrations are shown as dashed lines

Replacing $\bar{\Theta}$ *with* C using Eq (13.59) yields the connection between the net point-defect production rate and its mean concentration:

$$C = \left(\frac{kR_d^2}{2D}\right)\beta^2\left(\ln\beta - \tfrac{3}{4}\right) \tag{13.63}$$

The rate at which the dislocation line captures point defects is

$$J = D\left(\frac{dC'}{dr}\right)_{R_d} = \frac{D}{R_d}\left(\frac{kR_d^2}{2D}\right)\left(\frac{d\Theta}{d\eta}\right)_{\eta=1} = \frac{D}{R_d}\left(\frac{kR_d^2}{2D}\right)(\beta^2 - 1) \tag{13.64}$$

or, from Eq (13.63), in terms of C, Eq (13.64) is:

$$J = \frac{D}{R_d}\frac{\beta^2 - 1}{\beta^2}\frac{1}{\ln\beta - \tfrac{3}{4}}C \approx \frac{D}{R_d}\frac{1}{\ln\beta - \tfrac{3}{4}}C$$

The point defect absorption rates are $2\pi R_d J/\Omega$ per unit length of dislocation line and $2\pi R_d J\rho_d/\Omega$ per cm^3 of solid. Combining the latter rate with the flux J from the above equation yields the dislocation sink strength defined as:

$$k_{disl}^2 = \frac{2\pi\rho_d}{\ln\beta - \frac{3}{4}} = \frac{2\pi\rho_d}{\ln\left(\frac{R_{cell}}{R_d}\right) - \frac{3}{4}} = z\rho_d \ \ [\text{s}^{-1}] \tag{13.65}$$

The conventional derivation of the line sink strength, as given by Eq (13.46) and (13.47) (and Eq (13.93) of Ref.[6]), is missing the factor of ¾ in the denominator of Eq (13.65). The error incurred is 11% for $\beta = 10^3$ and 19% for $\beta = 10^2$. That is, as R_{cell} decreases, the dislocation lines are closer to each other and the error of treating them in isolation becomes more significant. For example for R_d = 1 nm, a dislocation density of 10^8 cm^{-2} implies β~560 while 10^{10} cm^{-2} implies β~ 56. Typical dislocation densities in engineering materials are on the order of 5 x 10^{19} cm^{-2}.

Spherical Sinks

The cubical unit cell for a cavity is approximated as a sphere of the same volume with the cavity at its center, as shown in the previous section. The sink strength of these cavities is governed by the diffusion equation of the mobile atomic-size species:

$$\frac{D}{r^2}\frac{d}{dr}\left(r^2\frac{dC'}{d\,r}\right) = -k \tag{13.66}$$

The cell radius R_{cell} is determined by Eq. (13.48). The boundary conditions are

$$C'\left(R_C\right) = 0 \quad \text{and} \quad \left(\frac{dC'}{d\,r}\right)_{R_{cell}} = 0 \tag{13.67}$$

As with the line sink, appropriate dimensionless terms are:

$$\eta = \frac{r}{R_C} \qquad \Theta = \frac{C'}{\left(kR_C^2/3D\right)} \qquad \beta = \frac{R_{cell}}{R_C} \tag{13.68}$$

In terms of which the solution to Eqs (13.66) and (13.67) is:

$$\Theta = \beta^3\frac{\eta-1}{\eta} - \tfrac{1}{2}(\eta^2-1) \tag{13.69}$$

The volume-averaged concentration is:

$$C = \frac{3}{4\pi(R_{cell}^3 - R_C^3)}\int_{R_C}^{R_{cell}} 4\pi r^2 C'(r)dr \quad \text{or} \qquad \overline{\Theta} = \frac{3}{\beta^3-1}\int_1^{\beta}\eta^2\Theta(\eta)d\eta \tag{13.70}$$

Substituting Eq (13.69)into Eq (13.70) yields:

$$\overline{\Theta} = \beta^3 + \tfrac{1}{2} - \frac{3}{\beta^3-1}\left(\tfrac{3}{5}\beta^5 - \tfrac{1}{2}\beta^3 - \tfrac{1}{10}\right) \approx \beta^2\left(\beta - \tfrac{9}{5}\right) \tag{13.71}$$

The second form retains the two highest-order terms in β. Converting from $\overline{\Theta}$ *to* C by means of Eq (13.68) gives:

$$C = \left(\frac{kR_C^2}{3D}\right)\beta^2\left(\beta - \tfrac{9}{5}\right) \tag{13.72}$$

The rate of absorption by a cavity is:

$$j_C = 4\pi R_C^2 D\left(\frac{d\,C'}{d\,r}\right)_{R_d} = 4\pi R_C^2\frac{D}{R_C}\left(\frac{kR_C^2}{3D}\right)\left(\frac{d\,\Theta}{d\,\eta}\right)_{\eta=1} = 4\pi R_C^2\frac{D}{R_C}\left(\frac{kR_C^2}{3D}\right)(\beta^3-1) \tag{13.73}$$

Combining the above two equations and multiplying by N_C cavities per cm^3 converts the rate from a per-cavity basis to a per-matrix atom basis and yields the void point defect absorption rate:

$$J^{void} = 4\pi R_C N_C DC \frac{\beta^3 - 1}{\beta^2(\beta - 9/5)} \tag{13.74}$$

For $\beta^3 >> 1$, t the cavity sink strength for both vacancy and interstitial is:

$$k_C^2 = 4\pi R_C N_C \frac{\beta}{\beta - 9/5} \tag{13.75}$$

If $\beta >> 9/5$, Eq (13.75) reduces to the conventional result given by Eq (13.55)

$$k_C^2 = 4\pi R_C N_C$$

Using $N_C \sim 4\times10^{13}$ cm^{-3} and $R_C \sim 2$ nm are typical of fission-gas bubbles in oxide fuel, so $\beta \sim 150$. The correction factor in Eq (13.74) is only ~ 1.01. However, for voids in a void lattice (Sect. 19.6.1) ($\beta \sim 6$), the correction factor is a non-negligible 1.45.

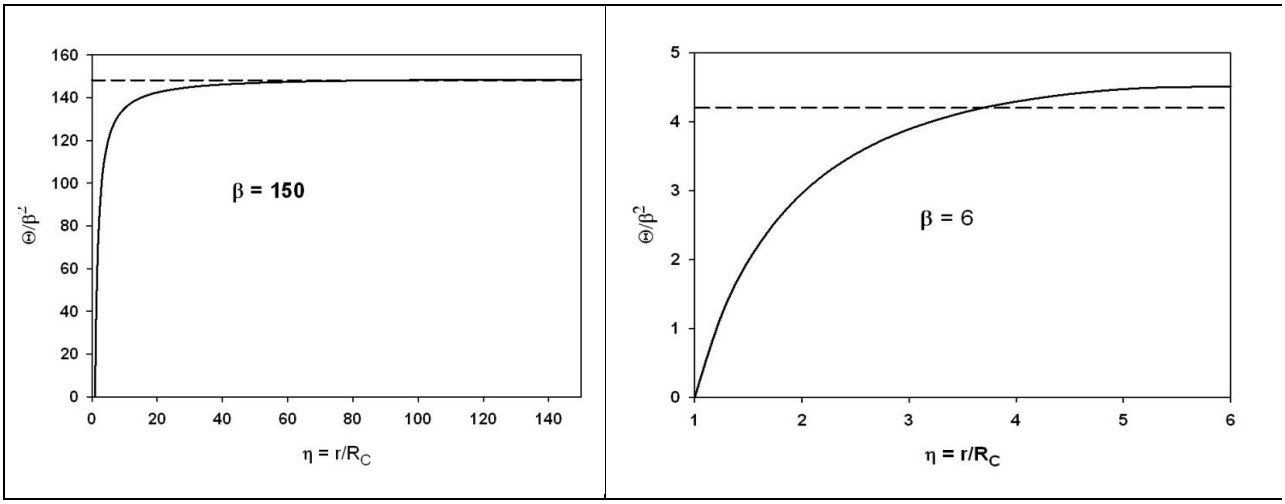

Fig. 13.11 Point-defect site fractions around cavities for two values of β. Volume-average values are shown as dashed lines

Figure 13.11 plots the dimensionless concentration against the dimensionless distance from the cavity surface. For large $\beta = R_{cell}/R_C$, the common assumption $C = C'(R_{cell})$ is perfectly adequate. This is true for most applications, such as bubbles in fuel and voids in metals. For small β (right hand graph) the above assumption is not acceptable, although such cases are uncommon.

13.6 Point Defect Balances

The point defects created during irradiation are the agents of microstructural evolution. Their migration through the lattice and subsequent annihilation at sinks, clustering or recombination is

the cause of macroscopic irradiation effects. This microstructure evolution is well described by a theory in which the point defect balances are calculated to result from defect creation and annihilation at various sinks, homogenized as in the derivations in the previous sections.

This so-called *rate theory*, was developed in the late 60s and early 70s [4] to explain void growth in irradiated metals. The theory is essentially a collection of point defect balance equations and their solutions. A brief summary of the theory is given in this section, and other summaries are also available in the literature [9, 10].

13.6.1 Point-defect Balance Equations

The overall change in the concentration of the defect species results from the balance between defect production, reaction and diffusion: :

Rate of Change = Generation rate- Diffusion - Recombination - Annihilation at sinks - Clustering

The rate equations for vacancies and interstitials are[1]:

$$\frac{\partial C_V}{\partial t} = D_V \nabla^2 C_V + k - K_{IV} C_I C_V - k_V^2 D_V C_V \tag{13.76}$$

$$\frac{\partial C_I}{\partial t} = D_I \nabla^2 C_I + k - K_{IV} C_I C_V - k_I^2 D_I C_I \tag{13.77}$$

where D_I and D_V are the defect diffusion coefficients, k is the generation rate in units of point defects per second per matrix atom (dpa/s),C_I and C_V are the point defect site fractions, and k_j^2 is the *total* sink strength for defect j (units of length^{-2}).

Equations (13.76) and (13.77) are solved with the appropriate boundary and initial conditions. If only spatially-average concentrations are needed, Eqs (13.76) and (13.77) are simplified to:

$$\frac{dC_V}{dt} = k - K_{IV} C_I C_V - k_V^2 D_V C_V \tag{13.78}$$

$$\frac{dC_I}{dt} = k - K_{IV} C_I C_V - k_I^2 D_I C_I \tag{13.79}$$

These forms of the balance equations are particularly useful for identifying the various stages of microstructure evolution.

For example assuming that the only sinks are cavities and dislocations, Eqs (13.46), (13.47) and (13.55)) the total sink strengths are:

$$k_I^2 = 4\pi N_C + z_I \rho_d \tag{13.80}$$

$$k_V^2 = 4\pi N_C + z_V \rho_d \tag{13.81}$$

[1] In addition, each cluster size requires a balance equation .

Note that the only difference between these two sink strengths is z_I and z_V, which differ by only ~ 2% (Example #2).

13.6.2 Steady-State Solutions of Point-Defect Balances

Given the previous formulation, the next step is to solve the defect balance equations for particular cases of interest. The quantities of interest are the average defect concentrations as functions of time, including t = ∞ (steady state), and the time to reach steady state. In the following we assume that one defect (interstitial) diffuses fast while the other (vacancy) is slow (a reasonable simplification in metals). The resulting coupled non-linear partial-differential equations have no analytical solution, and must be solved numerically. Because the coefficients in the equations often differ by several orders of magnitude, a robust equation solver is needed, and often the equations have to be non-dimensionalized in order to allow a stable numerical calculation.

The steady-state versions of Eqs (13.78) and (13.79) are:

$$0 = k - K_{IV} C_I C_V - k_V^2 D_V C_V \tag{13.82}$$

$$0 = k - K_{IV} C_I C_V - k_I^2 D_I C_I \tag{13.83}$$

Manipulating Eq (13.83) gives:

$$C_I = \frac{k}{K_{IV} C_V + k_I^2 D_I} \tag{13.84}$$

Inserting Eq (13.84) into (13.82) yields

$$C_V^2 + \frac{k_I^2}{K_{IV}} D_I C_V - \frac{k k_I^2 D_I}{K_{IV} k_V^2 D_V} = 0 \tag{13.85}$$

The solutions of which are:

$$C_V = -\frac{k_I^2 D_I}{2K_{IV}} \left[\frac{k k_I^2 D_I}{K_{IV} k_V^2 D_V} + \left(\frac{k_I^2}{4K_{IV}} \right)^2 \right]^{1/2} \tag{13.86}$$

Multiplying the first term in the brackets by $\frac{4(k_I^2 D_I)^2 K_{IV}}{4(k_I^2 D_I)^2 K_{IV}}$ and rearranging yields

$$C_V = \frac{k_I^2 D_I}{2K_{IV}} \left[\sqrt{1+\xi} - 1 \right] \tag{13.87}$$

$$C_I = \frac{k_V^2 D_V}{2K_{IV}}\left[\sqrt{1+\xi}-1\right] \tag{13.88}$$

where

$$\xi = \frac{4kK_{IV}}{k_I^2 k_V^2 D_I D_V} \tag{13.89}$$

is the dimensionless *defect annihilation number*, which measures the balance between defect production/recombination and annihilation at sinks[2].

Taking the limit where $\xi >> 1$ (equivalent to assuming that production/ recombination is much stronger than annihilation at sinks) makes the term in brackets in Eq. (13.87) and (13.88) approximately equal to $\xi^{1/2}$. In this *recombination- dominated regime*, the steady-state concentration s are:

$$C_V \simeq \frac{k_I^2 D_I}{2K_{IV}}\xi^{1/2} = \left(\frac{k_I^2 D_I k}{k_V^2 D_V K_{IV}}\right)^{1/2} \tag{13.90}$$

$$C_I \simeq \frac{k_V^2 D_V}{2K_{IV}}\xi^{1/2} = \left(\frac{k_V^2 D_V k}{k_I^2 D_I K_{IV}}\right)^{1/2} \tag{13.91}$$

When sinks are the main annihilation mechanism, $\xi << 1$ (so $(1+\xi)^{1/2} \simeq 1+\frac{\xi}{2}$. Using equation (13.89) it can be shown that the steady-state concentrations are:

$$C_V = \frac{k_I^2 D_I}{2K_{IV}}\frac{\xi}{2} = \frac{k}{k_V^2 D_V} \tag{13.92}$$

$$C_I = \frac{k_V^2 D_V}{2K_{IV}}\frac{\xi}{2} = \frac{k}{k_I^2 D_I} \tag{13.93}$$

Example #.3: Defect Concentration in Zr under Neutron Irradiation

Calculate the steady state defect concentrations for reactor temperature neutron irradiation of zirconium. Assume that T_{irr}=573 K, k=5x10^{-8} dpa/s, ρ_d = 10^{10} cm^{-2}, D_o = 0.01 cm^2/s. Consider that $E_m^V = 1.65eV$ *and* $1.0eV$ and $E_m^I = 0.1eV$ *and* $0.5eV$. Compare with the equilibrium defect concentrations if $E_f^V = 1.5eV; E_f^I = 3.0eV$. When will steady state be reached?

[2] Since k, K_{IV}, $k_V^2 D_V$ and $k_I^2 D_I$ are all in units of s^{-1}.

$D_I = 0.01 \times \exp(-0.1/8.62\times10^{-5}\times573)$ cm^2/s and likewise for the other diffusion coefficients.

$C_I = \dfrac{k}{z_I D_I \rho_d}$ which for 0.1 eV gives 3.7 x 10^{-15} and for 0.5 eV gives 1.2 x 10^{-11}

$C_V = \dfrac{k}{z_V D_V \rho_d}$ which for 1.0 eV gives 3.1 x 10^{-7} and for 1.65 eV gives 0.16

The characteristic time for interstitials to arrive at sinks is $t_I = 1/z_V\rho_d D_V$ =7.5 x 10^{-8} s and 2.4 x 10^{-4} s (interstitials arrive essentially instantaneously at sinks) and that for vacancies is $t_V = 1/z_i\rho_d D_i$=3.2 x 10^6 s and 6.2 s (for 1.65 and 1.0 eV migration energy, respectively). Note the significant influence of the migration and formation energies of the defects on their concentrations, and the large differences between vacancies and interstitials. However the value of 0.16 (16%) for the vacancy concentration is unphysical, as much before such a concentration is achieved the vacancy concentration is limited by mutual interaction and divacancy and higher order cluster formation.

The equilibrium defect concentrations at this temperature are C_V^{eq} =6.47 x 10^{-14} and C_I^{eq} = 4.2 x 10^{-27}. As expected the equilibrium defect site fractions are orders of magnitude lower than those under irradiation.

13.6.3. Transient Solutions: Kinetics of Defect Accumulation

To study the defect concentrations in the transient regime during irradiation of an initially defect-free solid to the final steady states derived above, we consider the transient accumulation of defects under the two regimes. The description adopted here is taken from Sizmann [10]. At the beginning, point defects are created in what is essentially a defect-free solid. The point defects are few and they do not interact with each other. During this stage the interstitial and vacancy concentrations both increase at the rate of production:

$$C_V = C_I = k\,t \tag{13.94}$$

This stage normally ends quickly, as defect interaction is strong. Depending on the microstructure of the material, the damage rate and the irradiation temperature, either defect elimination at sinks or recombination of interstitials and vacancies limits the accumulation expressed in Eq. (13.94). If defect absorption at sinks first limits accumulation, then we have a *sink-dominated* regime, whereas if defect recombination limits accumulation the regime is *recombination-dominated*.

Because interstitials and vacancies are homogeneously distributed throughout the material, the diffusion length the defects have to travel for recombination is much smaller than that for absorption at widely-separated sinks (low sink density). As a result, as the temperature decreases, the importance of recombination increases relative to thermally activated diffusion to far away sinks**.** In addition if the displacement rate is high, the defects have less time to arrive at sinks and therefore recombination is favored with respect to sink absorption. Finally as the sink density increases, the spacing between sinks decreases and consequently the distance defects have to

travel for absorption at sinks also decreases, causing sink absorption to become increasingly favored.

In summary, in situations where temperature is low, displacement rate is high, and sink density is low, *recombination* dominates. When the temperature is high, displacement rate is low and sink density is high, it is *absorption at sinks* that dominates microstructure evolution.

Recombination-Dominated Regime

Figure 13.12 shows a log-log plot of defect concentration versus time when the initial defect accumulation is limited by recombination.

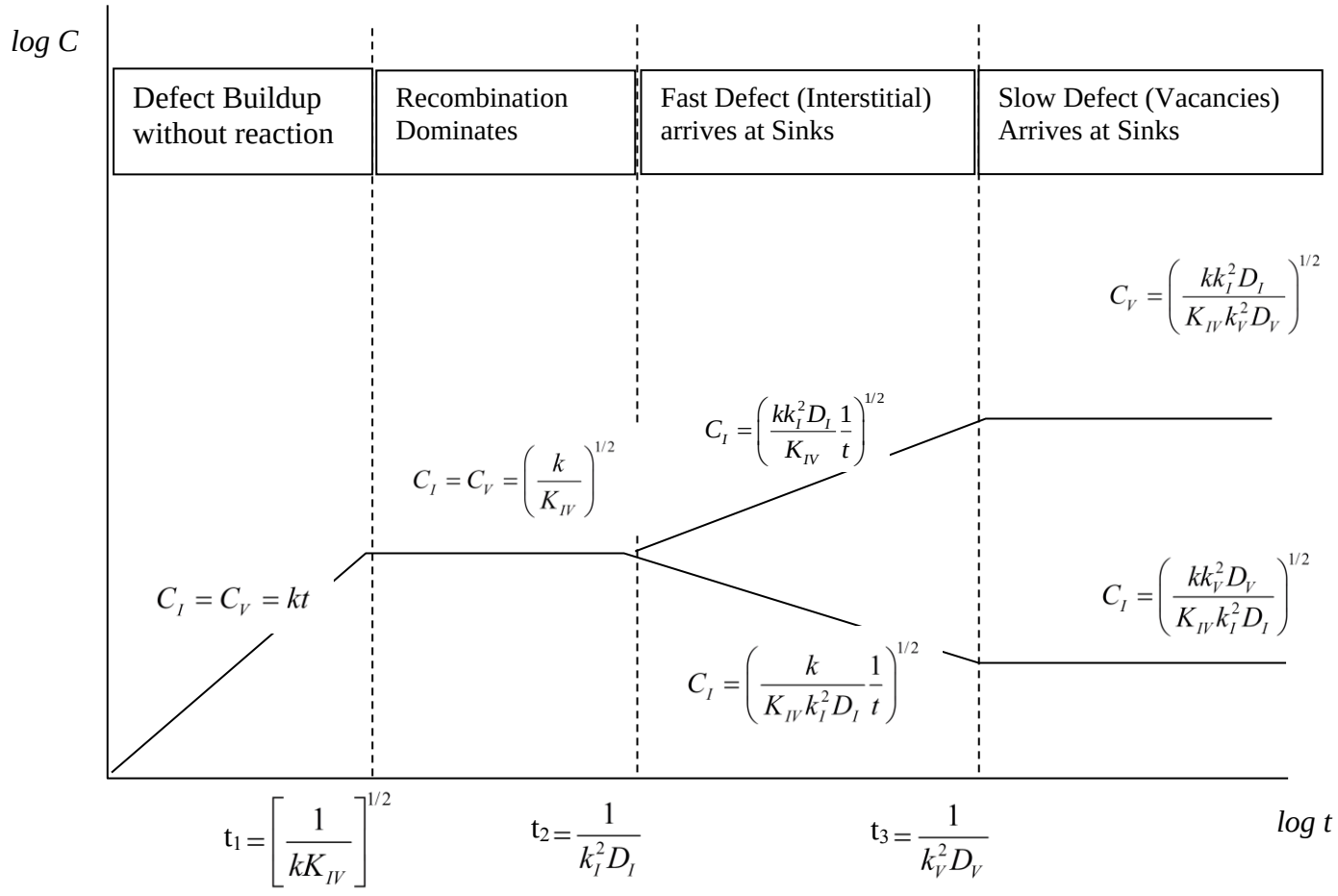

Figure 13.12: **Defect concentrations as functions of time in a recombination-dominated regime.**

The characteristic time for recombination to limit defect accumulation is obtained by setting the defect generation rate equal to the recombination rate

$$k = K_{IV} C_I C_V \tag{13.95}$$

Stage 1

During the first stage, Eq. (13.94) is valid. Substituting into Eq (13.95) and solving for the time gives the time for recombination to limit defect accumulation:

$$t_1 = \left(\frac{1}{k K_{IV}} \right)^{1/2} \tag{13.96}$$

After t_1, recombination exactly balances production and thus no further increases in defect concentrations occur. From Eqs (13.94) and (13.96), the defect concentrations are then frozen at

$$C_I = C_V = k\, t_1 = \left(\frac{k}{K_{IV}} \right)^{1/2} \tag{13.97}$$

Stage 2

If recombination were the only process for defect elimination, this would be the final steady state. However, sinks eventually influence defect accumulation. At time t_2 the fast defect (interstitial) starts to arrive in significant quantities at the defect sinks and C_I decreases. This leads to a decrease in the recombination rate and to a corresponding *increase* in vacancy concentration. The characteristic time for interstitial arrival at the sinks is found by setting

$$\frac{\partial C_I}{\partial t} = -\left(k_I^2 D_I \right) C_I \tag{13.98}$$

The characteristic time for this exponential process is

$$t_2 = \frac{1}{k_I^2 D_I} \tag{13.99}$$

This ushers in a period when interstitials arrive at sinks but vacancies do not, and during which the defect concentrations are given by:

$$C_V(t) = \left(\frac{k \left(k_{I,T}^2 D_I \right) t}{K_{IV}} \right)^{1/2} \tag{13.100}$$

$$C_I(t) = \left(\frac{k}{K_{IV} \left(k_{I,T}^2 D_I \right)\, t} \right)^{1/2} \tag{13.101}$$

Stage 3

The vacancy concentration builds up until, even with reduced mobility, they start arriving at sinks. By analogy with Eq. (13.99) this occurs at time t_3,

$$t_3 = \frac{1}{k_V^2 D_V} \quad , \tag{13.102}$$

After t_3 the flux of vacancies to sinks matches the interstitial flux. By substituting equation (13.102) into (13.101) and (13.100), in the final steady state the defect concentrations are:

$$C_I = \left(\frac{k k_V^2 D_V}{K_{IV} k_I^2 D_I} \right)^{1/2} \text{ and } C_V = \left(\frac{k k_I^2 D_I}{K_{IV} k_V^2 D_V} \right)^{1/2} \tag{13.103}$$

as found in Eqs (13.90) and (13.91).

Thus the respective defect concentration are related through their reaction rates with the sinks

$$\frac{C_V}{C_I} = \frac{k_I^2 D_I}{k_V^2 D_V} \tag{13.104}$$

In the case of neutral or nearly neutral sinks ($k_V^2 \cong k_I^2$) Eq (13.104) reduces to

$$D_I C_I = D_V C_V \tag{13.105}$$

That is, the ratio of defect concentrations is proportional to the inverse ratio of their diffusivities.

Example #4: Defect Accumulation regimes during neutron irradiation

Calculate the typical times of different stages of microstructure evolution and the times to steady state for the case of 293 K neutron irradiation of bcc Fe (lattice parameter= 0.28 nm) with a dislocation density of 10^8 cm^{-2}, and determine if we are in the recombination- dominated or sink-dominated regime. The vacancy and interstitial migration energies are 1.5 eV and 0.65 eV , respectively, the recombination number is 200, the displacement rate is 10^{-7} dpa/s and the vibration frequency is 10^{13} Hz.

For bcc Fe, Z=8 and the elemental jump distance is $a_o \frac{\sqrt{3}}{2}$ =0.24 nm

The diffusion coefficient is

$$D_I = \frac{8}{6} \times (2.44 \times 10^{-8})^2 \times 10^{13} \times \exp(-0.65 / 8.62 \times 10^{-5} \times 293) = 5.3 \text{ x } 10^{-14} \text{cm}^2/\text{s}$$

The vacancy diffusion coefficient is

$$D_V = \frac{8}{6} \times (2.44 \times 10^{-8})^2 \times 10^{13} \times \exp(-1.5 / 8.62 \times 10^{-5} \times 293) = 1.27 \times 10^{-28} \text{ cm}^2/\text{s}$$

and the recombination rate constant is

$$K_{IV} = 200 \times 10^{13} \times \exp(-0.65 / 8.62 \times 10^{-5} \times 293) = 1.33 \times 10^4 \, s^{-1}$$

the time for recombination is

$$t_1 = \frac{1}{\sqrt{k K_{IV}}} = \frac{1}{\sqrt{10^{-7} \times 1.33 \times 10^4}} = 274 s$$

The time for interstitials to arrive at the sinks is

$$t_2 = \frac{1}{z_I \rho_d D_I} = \frac{1}{1.02 \times 10^8 \times 5.3 \times 10^{-14}} = 1.86 \times 10^5 \, s = 51 h$$

The final steady state is reached *when vacancies arrive at the sinks*

$$t_3 = \frac{1}{z_v \rho_d D_v} = \frac{1}{10^8 \times 1.28 \times 10^{-28}} = 7.8 \times 10^{19}\, s = 2.48 \times 10^{12}\ \ years$$

Since this is longer than the age of the universe, steady state is not reachable by this mechanism. In this case, the concentration of vacancies continues to increase until their concentration is so high as to cause defect clustering (Sect 13.6).

Sink-Dominated Regime

If the defects are very mobile, the sink density high enough or if the displacement rate is low enough, defect accumulation is limited by absorption at sinks, which starts at time t_2

That is, the characteristic time t_2 defined in Eq (13.99) is shorter than t_1 defined in Eq (13.96). When interstitials start arriving at the defect sinks, their concentration reaches a quasi-steady state, in which the creation rate is equal to the elimination at the sinks. The concentration then levels off at a value.

$$C_I = k\, t_2 = \frac{k}{D_I k_I^2} \qquad (13.106)$$

This is the same as final steady state for interstitials derived before (Eq (13.93)).

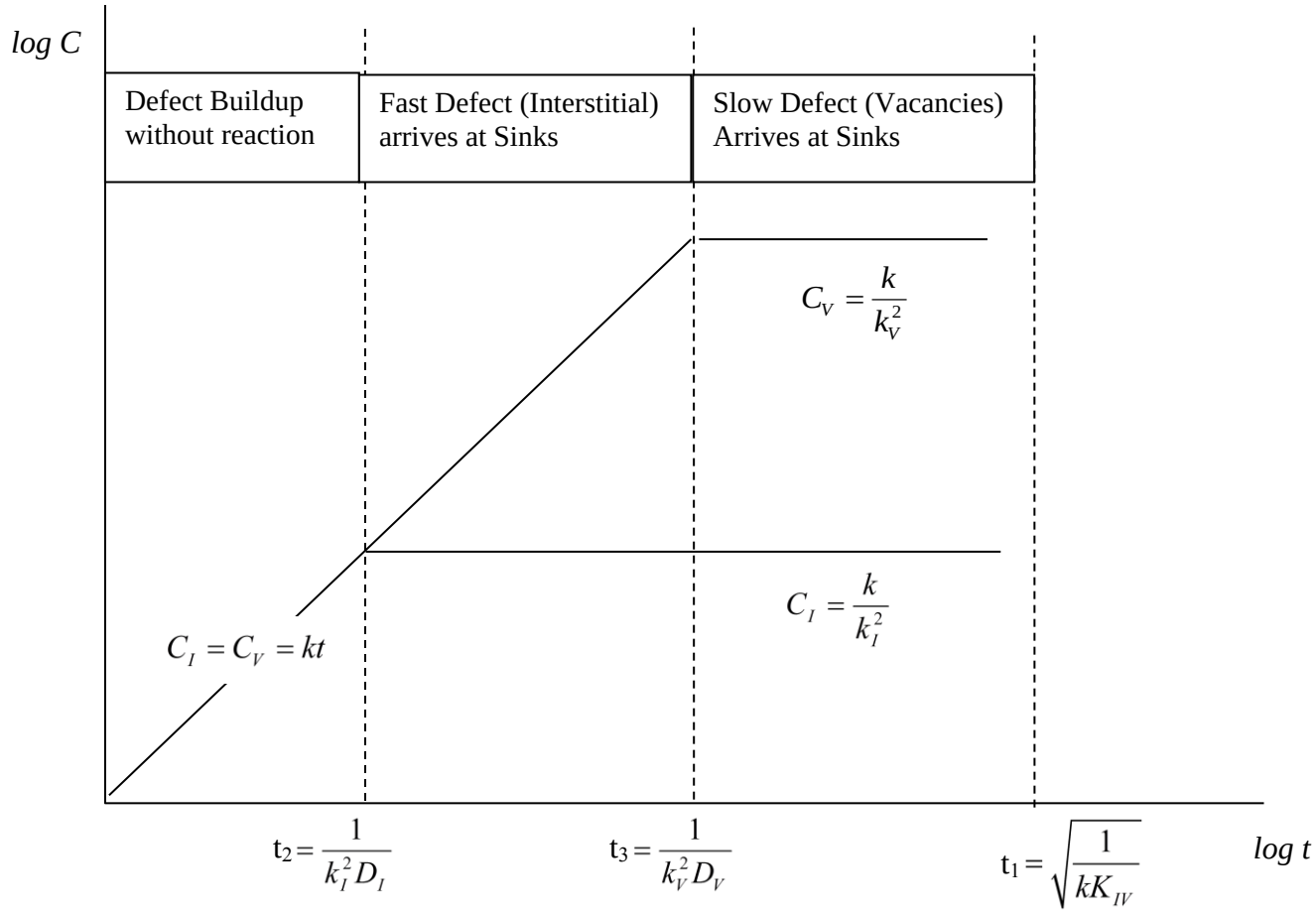

Figure 13.13: **Defect concentrations versus time under irradiation for a sink-dominated regime.**

The vacancies continue to increase until t_3 when they start arriving at sinks

$$C_V = k\, t_3 = \frac{k}{D_V k_V^2} \tag{13.107}$$

In the sink-dominated regime, the defect concentrations are proportional to the defect creation rate and inversely proportional to the sink density. For neutral sinks it is straightforward to show that equation Eq (13.105) is still valid.

13.7 Numerical and Approximate Solutions

The next step is to actually solve the point defect balance equations for particular cases to find the defect concentrations as functions of time. As stated above, the equations are coupled and non-linear and as a result they have no analytical solution, and must be solved numerically. As stated above, because the differences between the coefficients in the equations are often orders of magnitude, a robust equation solver is needed.

13.7.1. Non-dimensionalization and Numerical Solution

Equations (13.78) and (13.79) can be non-dimensionalized by:

$$\tau = \sqrt{kK_{IV}}\ t \qquad X = \sqrt{\frac{K_{IV}}{k}}C \tag{13.108}$$

$$\tau_V = \frac{\sqrt{kK_{IV}}}{k_V^2 D_V} \qquad \tau_I = \frac{\sqrt{kK_{IV}}}{k_I^2 D_I} \tag{13.109}$$

The point defect balance equations become:

$$\frac{dX_V}{d\tau} = 1 - X_V X_I - \frac{X_V}{\tau_V} \tag{13.110}$$

$$\frac{dX_I}{d\tau} = 1 - X_V X_I - \frac{X_I}{\tau_I} \tag{13.111}$$

Equations (13.110) and (13.111) can be solved numerically using Euler's method. The code, which can be used in a simple spreadsheet, is shown below.

1. *Input tau_V and tau_I*
2. *Input initial conditions: $X_V = X_I = 0$ at $\tau = 0$.*
3. *Input $\Delta\tau$*
4. *Start loop*
   - *$gradX_V = 1 - X_V X_I - X_V / tau_V$*
   - *$gradX_I = 1 - X_V X_I - X_I / tau_I$*
   - *$X_V = X_V + gradX_V \times \Delta\tau$*
   - *$X_I = X_I + gradX_I \times \Delta\tau$*
   - *$\tau = \tau + \Delta\tau$*
   - *write τ, X_V and X_I*
   - *if $\tau < \tau_{max}$ return to step 4*
5. *exit*

The above numerical solution reproduces reasonably well the plots in Figs. 13.12. An example of such a calculation is shown in Figure 13.14. For this example, $k = 10^{-2}$ dpa/s, $D_I = 1.35 \times 10^{-7}$ cm^2/s, $D_V = 9.4 \times 10^{-13}$ cm^2/s, $K_{IV} = z_{IV} D_I / a_o^2 = 7.49 \times 10^{10}$, $\Delta\tau = 10^{-2}$. With these parameters the time constants in the solutions proposed by Sizmann above can be verified.

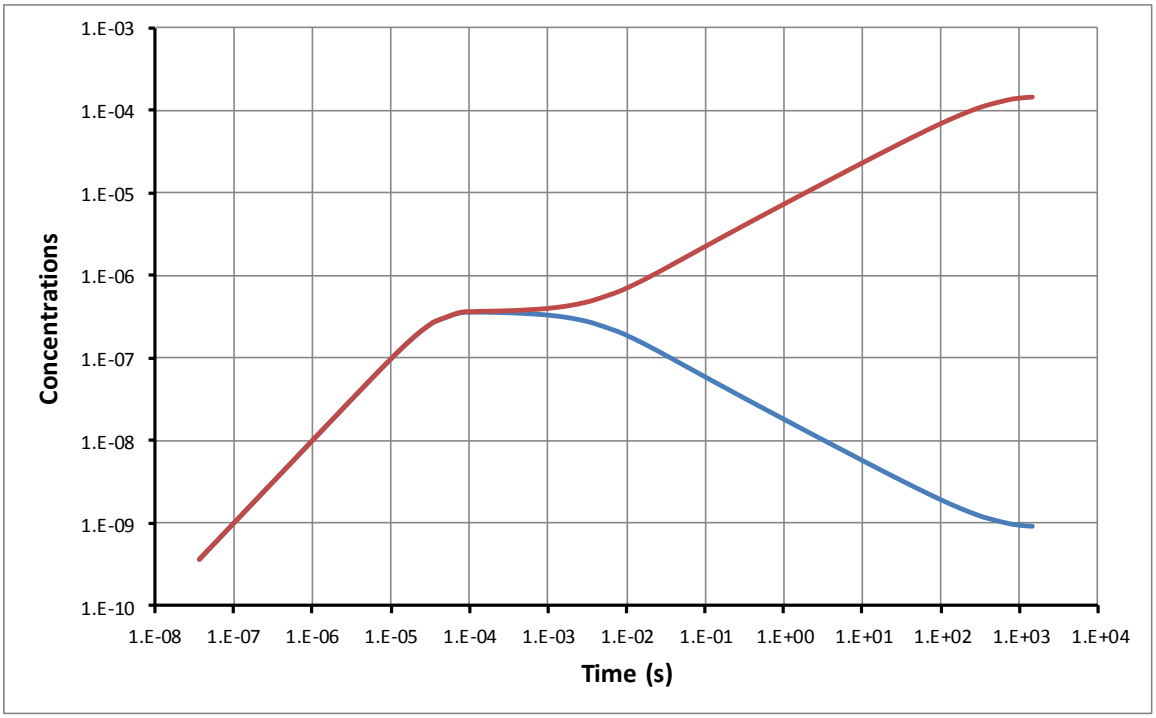

Fig. 13.14 Numerical solutions for point defect concentrations. The interstitials are the blue curve while the vacancies are the red curve.

For example t_1 (time for recombination to limit point defect accumulation) is ($1/\sqrt{kK_{IV}}$), which is = 3.5 x10^{-5} s which corresponds well with the calculation. The time for interstitials to arrive at sinks is

$$t_2 = 1/k_{I,tot}^2 D_I$$

which in this case is 5 x 10^{-3} s, which also corresponds well with the time at which the interstitial and vacancy curves split. The time for vacancies to arrive at sinks (time t_3) is 795 s, which corresponds to the final steady state at which the curves level off. The calculated final steady-state concentrations from are C_I=9.2 x 10^{-10} and C_V=1.45x 10^{-4} which also correspond well to the calculated values from Eqs (13.90) and (13.91) of 9.21x10^{-10} and 1.45 x10^{-4}.

13.7.2. Approximate solutions for limiting cases

Recombination-Dominated Regime

In this regime, the sink absorption terms are neglected. In what remains, $C_V = C_I = C$ and

$$\frac{dC}{dt} = k - K_{IV}C^2 \qquad (13.112)$$

This equation is non-dimensionalized by:

$$\tau = \sqrt{kK_{IV}}\, t \qquad\qquad X = \sqrt{\frac{K_{IV}}{k}}\, C \tag{13.113}$$

which converts Eq (13.112) to:

$$\frac{dX}{d\tau} = 1 - X^2 \tag{13.114}$$

For which the solution, subject to X = 0 at τ = 0, is:

$$X = \frac{1-e^{-2\tau}}{1+e^{-2\tau}} \quad or \quad C_V = \sqrt{\frac{k}{K_{IV}}}\left(\frac{1-e^{-2\sqrt{kK_{IV}}\,t}}{1+e^{-2\sqrt{kK_{IV}}\,t}}\right) \tag{13.115}$$

Equation (13.115) is plotted in Fig. 13.16.

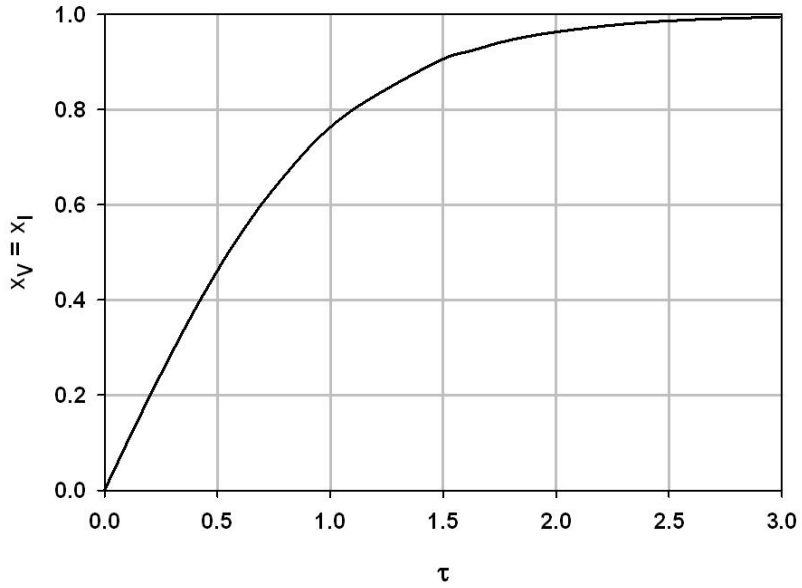

Fig. 13.16. Point-defect concentration versus time for recombination-dominated conditions

The approximate solution reproduces the previously described defect accumulation behavior, in that initially the two point-defect concentrations grow linearly with time, or $X = \tau$,, but as $\tau \rightarrow 1$, the concentration begins to level off at $X_{SS} = 1$.

Example #5 Recombination-Dominated Regime: Neutron irradiation of iron at 293 K

$\rho_d = 10^8$ cm^{-2}; k = 10^{-7} dpa/s; $D_I = 5\times10^{-14}$ cm^2/s; $D_V = 1.3\times10^{-28}$ cm^2/s; $Z_{IV} = 200$
$a_o = 0.24$ nm. From Eq

$$K_{IV} = \frac{z_{IV} D_I}{a_o^2} = \frac{(200)(5\times10^{-14})}{(2.4\times10^{-8})^2} = 1.7\times10^4\ s^{-1}$$

Because no cavities are present, the sinks are the dislocations ($z_I \sim 1$)

The ξ factor Eq. (13.89) is very large, indicating a recombination- dominated regime for which (13.109)

$$\tau_I = \frac{\sqrt{(10^{-7})(1.7\times10^{4})}}{(10^{8})(5\times10^{-14})} = \frac{0.04}{5\times10^{-6}} = 8\times10^{3}$$

$$\tau_V = \frac{0.04}{(10^{8})(1.3\times10^{-28})} = 3\times10^{18}$$

These are the characteristic times for the two point defects to reach the dislocation sink. Converting to real times using Eq (13.108)

$$t_I = \frac{\tau_I}{\sqrt{kK_{IV}}} = \frac{8\times10^{3}}{0.04} = 2\times10^{5}\ s \qquad \text{and} \qquad t_V = \frac{\tau_V}{\sqrt{kK_{IV}}} = \frac{3\times10^{18}}{0.04} = 6\times10^{20}\ s$$

steady-state is not reached. Once t_I is passed (a little over 2 days), defect accumulation proceeds according to Eqs (13.100) and (13.101), that is, the interstitial concentration *decreases* as $t^{1/2}$ and vacancies *increase* as $t^{1/2}$.

Sink-Dominated Regime

If the defects are very mobile and the sink density is high or if the displacement rate is low, then the effect of recombination is minimal. This can be best seen using the dimensionless forms shown in Eqs (13.110) and (13.111). Since $D_I >> D_V$, Eq (13.109) implies $\tau_I << \tau_V$. If in addition $\tau_I << 1$, for the last term on the right of Eq(13.111) to remain of order unity, X_I must be << 1. Therefore, this equation simplifies as follows

- because X_V is of order unity, $X_V X_I << 1$
- because X_I is small, $dX_I/d\tau << 1$

Equation (13.111) simplifies to:

$$X_I = \tau_I \tag{13.116}$$

Substituting this result into Eq. (13.110)

$$\frac{dX_V}{d\tau} = 1-(\tau_I + 1/\tau_V)X_V \cong 1 - X_V/\tau_V \tag{13.117}$$

integrating gives the vacancy concentration in the initial regime:

$$X_V = \tau_V\left(1-e^{-\tau/\tau_V}\right) \quad or \quad C_V = \frac{k}{k_V^2 D_V}(1-e^{-k_V^2 D_V t}) \tag{13.118}$$

Example # 6a Calculation of point defect concentrations during neutron irradiation of copper at 773 K

The point-defect diffusivities in copper at 773 K are (Ref. 1, p. 179):
$D_V = 5\times10^{-6}$ cm^2/s and $D_I = 7\times10^{-2}$ cm^2/s
also:
$\rho_d = 10^9$ cm^{-2} and k = 10^{-7} dpa/s; $z_I = 1.02$
The void sink strength is arbitrarily set at 0.5×10^9 cm^{-2}.
For a jump distance of 0.3 nm and $z_1z_2 = 500$, Eq (13.12) gives:

$$K_{IV} = \frac{z_{IV}D_I}{a_o^2} = \frac{(500)(7\times10^{-2})}{(3\times10^{-8})^2} = 4\times10^{16}\ s^{-1}$$

The regime can be inferred from the magnitude of ξ (Eq (13.89)):

$\xi = \dfrac{4\times10^{-7}\times4\times10^{16}}{(1.5\times10^9)^2\times5\times10^{-6}\times7\times10^{-2}} =$ 5.1x10^{-3}, indicating this is a *sink-dominated* regime, which means that the steady-state concentrations are given by Eqs (13.92) and (13.93). With the property values above we obtain C_v=1.3 x 10^{-11} and C_I=9.5 x10^{-16},

Eq (13.41) yields:

$$\tau_V = \frac{(4\times10^{16}\times10^{-7})^{1/2}}{(1.5\times10^9)(5\times10^{-6})} = 8.3 \qquad \tau_I = \frac{(4\times10^{16}\times10^{-7})^{1/2}}{(1.52\times10^9)(7\times10^{-2})} = 5.9\times10^{-4}$$

With the above property values, Eqs (13.116) and (13.118) are plotted in Fig. 13.15.
Steady-state X_I is attained at a time (τ_I) too short to be seen on the plot.
The steady-state vacancy concentration $(X_V)_{SS} = 10$ is achieved at $\tau_V \sim 8$, or in dimensional terms:

$$t_V = \frac{\tau_V}{\sqrt{kK_{IV}}} = \frac{8}{\sqrt{(10^{-7})(4\times10^{16})}} = 1.2\times10^{-4}\ s$$

$$(C_V)_{SS} = \sqrt{\frac{k}{K_{IV}}}(X_V)_{SS} = \sqrt{\frac{10^{-7}}{4\times10^{16}}}\times(10) = 1.6\times10^{-11}$$

$$(C_I)_{SS} = \sqrt{\frac{k}{K_{IV}}}(X_I)_{SS} = \sqrt{\frac{10^{-7}}{4\times10^{16}}}\times5.9\times10^{-4} = 10^{-15}$$

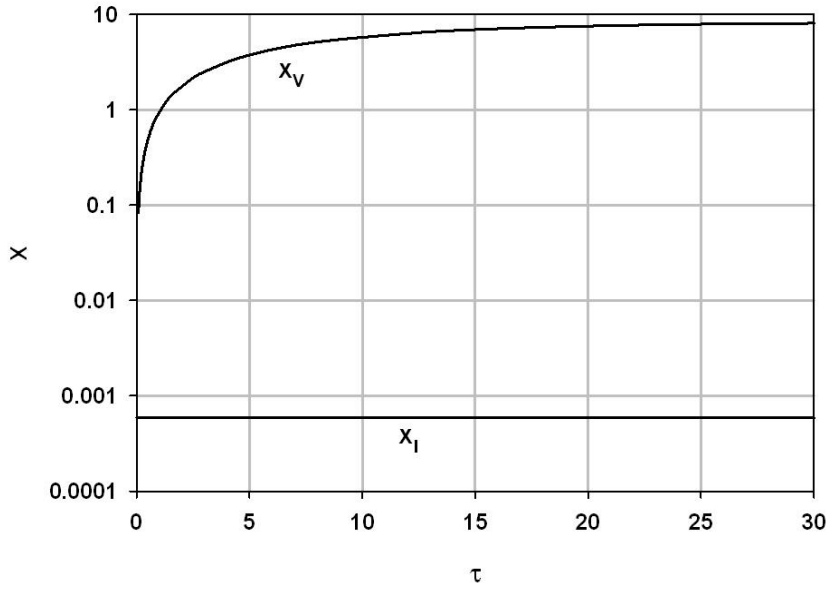

Fig. 13.15. Point-defect concentration variation with time for τ_V =8.3 $\tau_I = 6\times10^{-4}$

Example #6b Sink Dominated: neutron irradiation of zirconium at 573 K

$\rho_d = 10^{10}$ cm^{-2}; k = 5×10^{-8} dpa/s; $D_I = 1.3\times10^{-3}$ cm^2/s; $D_V = 1.6\times10^{-11}$ cm^2/s
Point-defect energies of formation: vacancies:1.32 eV; interstitials: 2.74 eV
Calculate characteristic times and steady-state concentrations
Since there are no cavities, $k_I^2 = k_V^2 = \rho_d$
Eliminate $\sqrt{kK_{IV}}$ from Eq (13.109) using τ from Eq (13.108)

$$t_I = \frac{1}{\rho_d D_I} = \frac{1}{(10^{10})(1.3\times10^{-3})} = 8\times10^{-8}\ s \qquad t_V = \frac{1}{\rho_d D_V} = \frac{1}{(10^{10})(1.6\times10^{-11})} = 6\ s$$

In this regime the steady-state concentrations are equal to the tau times.
Equate X from Eq (13.109) with X from Eq (13.108) to give:

$$C_I = \frac{k}{\rho_d D_I} = \frac{5\times10^{-8}}{(10^{10})(1.3\times10^{-3})} = 4\times10^{-15} \qquad C_V = \frac{k}{\rho_d D_V} = \frac{5\times10^{-8}}{(10^{10})(1.6\times10^{-11})} = 3\times10^{-7}$$

Equilibrium concentrations:

$$C_I^{eq} = \exp\left(-\frac{2.74}{8.62\times10^{-5}\times573}\right) = 4\times10^{-27} \qquad C_V^{eq} = \exp\left(-\frac{1.32}{8.62\times10^{-5}\times573}\right) = 2\times10^{-13}$$

As expected, these are many orders of magnitude lower than the site fractions due to irradiation.

For a different pair of diffusivities (D_I=2.5x10^{-1} cm^2/s, D_V=2.5x10^{-7} cm^2/s) , the calculated point-defect site fractions are:

$C_I = 2\times10^{-13}$ *and* $C_V = 0.2$

In this case the approximation of isolated defect accumulation is no longer adequate because the large calculated value of C_V implies that divacancy formation should be included.

13.7.3. Grain-boundary sink strength

Planar sinks such as free surfaces and grain boundaries can also substantially affect microstructure evolution under irradiation. Unlike dislocations, grain boundaries are *neutral* sinks, i.e. the same for both types of point defects. Having determined the steady- state point-defect concentrations, at the sink strength of grain boundaries, k_{gb}^2, can be .calculated.

As before, steady state and no recombination are assumed. As shown in Fig. 13.17, the grain is divided into two zones. In the inner zone, Eqs (13.92) and (13.93) apply, giving the following point-defect concentrations:

$$C_V = \frac{k}{k_V^2 D_V} \; and \; C_I = \frac{k}{k_I^2 D_I} \tag{13.119}$$

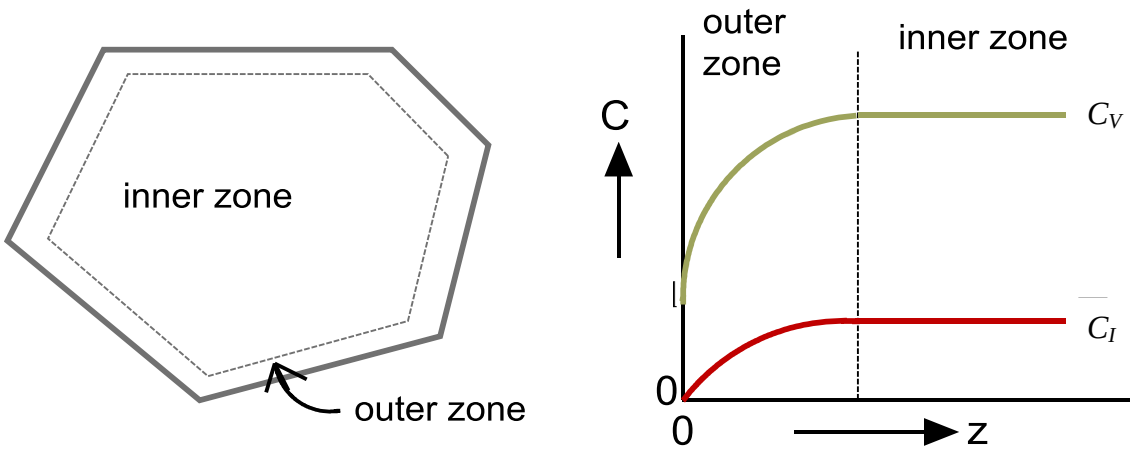

Fig. 13.17 Partitioning of grain for calculation of grain-boundary sink strength

In the outer zone, bordering the grain boundary, the same simplifications apply, but terms accounting for concentration gradients from C_V *to* C_V^{eq} *and* C_I *to* 0 are added to the simplified point-defect balance equations. For vacancies Eq (13.78) becomes:

$$D_V \frac{d^2 \mathcal{C}_V}{d\,z^2} + k = k_V^2 D_V \mathcal{C}_V \tag{13.120}$$

and a similar equation for interstitials. The solution of Eq (13.120) is

$$\mathcal{C}_V(z) = Ae^{-\sqrt{k_V^2}z} + Be^{\sqrt{k_V^2}z} + \frac{k}{k_V^2 D_V} \tag{13.121}$$

The following boundary conditions apply:
$\mathcal{C}_V$ must be finite as z $\rightarrow\infty$, so B = 0
According to Eq (13.119) the last term is the bulk site fraction C_V
At the grain boundary $\mathcal{C}_V(0) = 0$, so $A = -C_V$
Inserting the above into Eq (13.121) gives the solution:

$$\frac{\mathcal{C}_V(z)}{C_V} = 1 - e^{-\sqrt{k_V^2}z} \tag{13.122}$$

The flux of vacancies to the grain boundary is:

$$J_{V\to gb} = \left(4\pi R_{gr}^2\right) D_V \left[\frac{d\left(\mathcal{C}_V\right)}{dz}\right]_{z=0} = \left(4\pi R_{gr}^2\right) D_V \sqrt{k_V^2} C_V \tag{13.123}$$

R_{gr} is the equivalent radius of the grain.

The vacancy sink term in Eq (13.119) $k_{gb}^2 D_V$ represents the rate of vacancy absorption by the grain boundaries per matrix atom (units s^{-1}). From Eq (13.122), the concentration gradient at the grain boundary is $k_V C_V$ so:

$$k_{gb}^2 D_V C_V = \frac{J_{V\to gb}}{\frac{4}{3}\pi R_{gr}^3} = \frac{3\sqrt{k_V^2} D_V C_V}{R_{gr}}$$

from which the grain-boundary sink strength is:

$$k_{gb}^2 = \frac{3\sqrt{k_V^2}}{R_{gr}} \tag{13.124}$$

Table 13.1 lists two features of the grain-boundary sink strength for typical values of the strength of the extended sinks (dislocations plus cavities, Eq (13.81)).

Table 13.1 Characteristics of the grain-boundary sink strength for a 10 μm diameter grain

k_V^2, cm^{-2}	k_{gb}^2 / k_V^2	$1/\sqrt{k_V^2}, \mu m$
10^{11}	0.02	0.03
10^{10}	0.06	0.10
10^{9}	0.20	0.31

The second column gives the ratio of the strengths of the grain-boundary and intragranular sinks. For large $k_{V,T}^2$ the ratio is less than 10%, which means that the grain-boundary sink can safely be neglected in the point-defect analysis. However, when the strength of the intragranular sinks is 10^9 cm^{-2} or less, the ratio is > 20%. For such relatively clean crystals, the grain boundary sink term $k_{gb}^2 D_V C_V$ *and* $k_{gb}^2 D_I C_I$ should be added to the right-hand sides of the point defect balances. Also, the grain-boundary sink effect becomes larger the smaller the grain size.

There is really no sharp separation between the inner and outer regions of the grain as shown in Fig. 13.17. However, according to Eq (13.122) the concentration in the outer zone reaches $1 - e^{-1}$ of the inner value at a distance $1/\sqrt{k_V^2}$ from the grain boundary. These characteristic lengths are listed in the last column of Table 13.1. They are to be compared to the grain radius, which is

5 μm for the Table. The characteristic lengths do not exceed 0.3 μm, which in most cases is sufficiently smaller than the grain radius that the two-zone approximation is valid.

13.8 Rate Theory Limitations

Several approximations were made in these derivations, and more sophisticated versions of rate-theory modeling take some of these effects into account. There are also other classes of models for microstructure evolution under irradiation, including the production bias model (Sect. 19.6) [11] which takes into account the spatial and temporal correlation of damage production. In the last few years there has been an increase in the use of powerful numerical techniques including Kinetic Monte Carlo and Cluster dynamics simulations of microstructure evolution (Chap 14). Because of computer limitations, these methods are for the moment[3] restricted to the description of the early stages of radiation damage and microstructure evolution (100s of picoseconds). However, their ranges of applicability are bound to increase as computers become more powerful, and can perform enough histories to create an average picture of the evolution of the microstructure. Currently, limitations on computer power do not allow an extension of these calculations to the time domains where thermal diffusion can be simulated.

We review in the following some of the revisions that can be performed within the framework of the rate-theory formulation presented here. One of the most obvious additions is the formation of as vacancy clusters or defects trapped at solute impurities. In this case, additional balances are needed to be solved simultaneously with the point-defect balances (e.g., irradiation-induced segregation in Chap. 24).

To evaluate the characteristic time for divacancy formation to significantly affect microstructure evolution we set

$$\frac{\partial C_V}{\partial t} = -K_{VV} C_V^2 \tag{13.125}$$

which yields the characteristic time for di-vacancy formation t_5:

$$t_5 = \left[\frac{K_{IV}}{k k_V^2 D_I K_{VV}^2} \right]^{1/3} \tag{13.126}$$

if τ_5 is smaller than any of the times t_1-t_4 above, then divacancy formation needs to be considered. For example, in example #, for an interstitial migration energy of 0.5 eV and a vacancy migration energy of 1.0 eV, t_5 = 74 s, which means that divacancy formation needs to be considered, as had also been inferred by the large vacancy concentrations achieved when this process is neglected.

If the features in the microstructure evolve with time (e.g., sinks are created, their strength varies), then more sophisticated versions of the sink strengths have to be derived.

[3] As of 2014

Problems

13.1. An iron component in a nuclear reactor core is subjected to a fast flux of 5 x 10^{13} neutrons.$cm^{-2}s^{-1}$ at an average energy 1 MeV. The defects created are eliminated only by recombination and by absorption at dislocations. The dislocation density is constant at ρ_d = $10^{10}cm^{-2}$, the interstitial migration energy is 0.5 eV and the vacancy migration energy is 1 eV.

a. Calculate the interstitial and vacancy concentrations at steady state.
b. Find the time to reach steady state.
c. Compare these with electron irradiation at room temperature. Take the k_{el} = 5 x 10^{-3} dpa.s^{-1}, and assume an infinite medium similar to the above.

Make reasonable estimates of any needed parameters.

13.2. Self-diffusion in U metal occurs by a vacancy mechanism. The diffusion coefficient is $D = D_O \exp(-E_{mv}/kT)$ where E_{mv} is the vacancy migration energy in U.

a. What is the self-diffusion coefficient of U in the absence of irradiation? The formation energy of vacancies is E_{fv}.

b. During irradiation Frenkel pairs are created at a rate *k (dpa/s)*, and only destroyed by recombination. What is the steady state vacancy concentration? What is the uranium self-diffusion coefficient by a vacancy mechanism under irradiation?

c. The interstitial migration energy is E_i. Sketch the variation of ln D_u vs. 1/T, identifying significant portions of the curve.

13.3. A thin foil thickness L is under irradiation. It is desired to calculate the strength of the surface sink. Assume that at the midplane of the foil the concentration is equal to the bulk concentration of defects C.

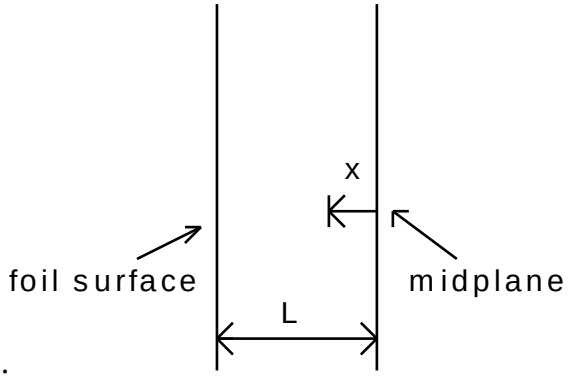

.

If the interstitial diffusion coefficient is D_i solve the diffusion equation for the plate geometry and obtain the flux of interstitials to the surface and identify the rate constant for annihilation of defects at the surface $k^2_{dis,I}$ and $k^2_{dis,V}$. Neglect defect generation.

13.4. In section 13.3 we calculated the rate of divacancy formation by considering the reaction of two vacancies in the fcc lattice.

$$V + V \xleftrightarrow{K_{vv}^{fcc}} V_2$$

In that calculation we multiplied the number of configurations from which the reaction can occur by the jump probability. Repeat the calculation for the hexagonal close-packed lattice, that is calculate K_{vv}^{hcp}. Assume that vacancy diffusion occurs between nearest-neighbors in the hcp structure. The vacancy migration energy is E_m^v and the vibration frequency is ν.

13.5. The reaction rates for reactions between defects and extended sinks were found in this chapter by solving the appropriate diffusion equations. It is also possible to derive these reaction rates by considering a certain fraction of the sites in the solid will be at the surface of extended sinks and that these sites are accessible via other nearest neighbor sites in a manner similar to what was done in the divacancy derivation section 13.4.

a) Derive the dislocation reaction rate using this method and compare to equations 13.%%. Can you explain the differences?

b) Derive the void reaction rate using this method and compare to equations 13.%%. Can you explain the differences?

13.9 References

[1] R. E. Stoller, "1.11 - Primary Radiation Damage Formation," in *Comprehensive Nuclear Materials*, R. J. M. Konings, Ed., ed Oxford: Elsevier, 2012, pp. 293-332.
[2] G. J. Dienes and G. H. Vineyard, *Radiation Effects in Solids*. New York: Interscience Publishers, 1957.
[3] M. J. Makin, "A simple theory of loop formation and enhanced diffusion in crystals examined by high voltage electron microscopy," *Philosophical Magazine*, vol. 20, pp. 1133-46, 1969.
[4] A. D. Brailsford and R. Bullough, "The rate theory of swelling due to void growth in irradiated metals," *Journal of Nuclear Materials*, vol. 44, pp. 121-135, 1972/8 1972.
[5] H. Wiedersich, *Radiation Effects*, vol. 12, p. 111, 1972.
[6] D. R. Olander, *Fundamental Aspects of Nuclear Reactor Fuel Elements*: ERDA, 1976.
[7] S. I. Golubov, A. V. Barashev, and R. E. Stoller, "1.13 - Radiation Damage Theory," in *Comprehensive Nuclear Materials*, R. J. M. Konings, Ed., ed Oxford: Elsevier, 2012, pp. 357-391.
[8] M. R. Hayns, "The role of bulk recombination in the theory of void swelling," *Journal of Nuclear Materials*, vol. 79, pp. 323-37, 02/ 1979.
[9] G. S. Was, *Fundamentals of Radiation Materials Science*. New York: Springer, 2007.
[10] R. Sizmann, "Effect of Radiation Upon Diffusion in Metals," *J. Nucl. Mater.*, vol. 69-70, pp. 386-412, 1978.
[11] C. H. Woo, A. A. Semenov, and B. N. Singh, " Analysis of Microstructural Evolution Driven by Production Bias," *Journal of Nuclear Materials*, vol. 206, pp. 170-199, 1993.